9-3-2013

# Second law analysis of a waste heat recovery combined power cycle using transcritical carbon dioxide

Robert Cordova

Robert Samuel Cordova
Candidate

Mechanical Engineering
Department

This thesis is approved, and it is acceptable in quality and form for publication:

*Approved by the Thesis Committee:*

Dr. Arsalan Razani , Chairperson

Dr. Randall Truman

Dr. Svetlana Poroseva

# SECOND LAW ANALYSIS OF A WASTE HEAT RECOVERY COMBINED POWER CYCLE USING TRANSCRITICAL CARBON DIOXIDE

**by**

**ROBERT SAMUEL CORDOVA**

**BACHELOR OF SCIENCE IN MECHANICAL ENGINEERING UNIVERSITY OF NEW MEXICO, 2010**

THESIS

Submitted in Partial Fulfillment of the
Requirements for the Degree of

**MASTER OF SCIENCE**
**MECHANICAL ENGINEERING**

The University of New Mexico
Albuquerque, New Mexico

**July 2013**

# SECOND LAW ANALYSIS OF A WASTE HEAT RECOVERY COMBINED POWER CYCLE USING TRANSCRITICAL CARBON DIOXIDE

**by**

**Robert Samuel Cordova**

**B.S., Mechanical Engineering, University of New Mexico, 2010**

**M.S., Mechanical Engineering, University of New Mexico, 2013**

## ABSTRACT

Common power cycles discard a large portion of useful energy into the environment via exhaust gasses. Through the use of cascade bottoming cycles, this wasted exergy may be utilized for power generation and hot water production. Heat transfer between cycles occurs through a heat exchanger. To maximize heat exchanger effectiveness, a transcritical working fluid is used in the Rankine bottoming cycle to better match the heating curve of the sensible heat source. Carbon dioxide is selected as the working fluid because it possesses a relatively low critical temperature which makes it attractive for low temperature waste heat applications. In contrast to many other working fluids, carbon dioxide is inert, abundant, non-flammable, and presents negligible environmental impact. The topping cycle to be used is an air Brayton cycle with methane as the fuel source. The purpose of this study is to quantify the performance of the transcritical bottoming cycle and the combined cycle as a whole by altering system parameters to gain insight for future research in the field of waste heat recovery.

# Table of Contents

# List of Figures

# List of Tables

# Nomenclature

| | | | |
|---|---|---|---|
| h | Enthalpy | $\Delta T_{HOT}$ | GH hot side temperature difference |
| s | Entropy | $\Delta T_{COLD}$ | GH cold side temperature difference |
| T | Temperature | $\Delta P$ | Relative pressure loss |
| $T_{ref}$ | Reference temperature | dS | Entropy change |
| $\bar{T}_{add}$ | Average temperature of heat addition | $dS_i$ | Entropy change from internal effects |
| $\bar{T}_{reject}$ | Average temperature of heat rejection | $dS_e$ | Entropy change from external effects |
| k | Ratio of specific heats | $\eta_1$ | First Law efficiency |
| E | Exergy | $\eta_2$ | Second Law efficiency |
| $R_P$ | Pressure Ratio | $\eta_R$ | Regenerator effectiveness |
| $\dot{m}$ | Mass flow rate | $\eta_C$ | Compressor isentropic efficiency |
| $V_{DOMESTIC}$ | Volumetric flow rate of domestic water | $\eta_P$ | Pump isentropic efficiency |
| TIP | Turbine inlet pressure | $\eta_{1CC}$ | Combined cycle 1st Law efficiency |
| TIT, $T_{MAX}$ | Turbine inlet temperature | $\dot{Q}_{in}$ | Rate of heat transfer into system |
| TET | Turbine exit temperature | $\dot{Q}$ | Heat transfer rate |
| DOE | Department of Energy | $\dot{W}_{net}$ | Net power output |
| BTU | British Thermal Unit | $\dot{E}_{fuel}$ | Rate of exergy addition from fuel |
| quad | Quadrillion BTUs | $\dot{E}_D$ | Component exergy destruction |
| GH | Gas heater | $\dot{E}_{flow}$ | Exergy flow across control volume |
| HX | Heat exchanger | | |
| HRSG | Heat Recovery Steam Generator | **Greek Letters** | |
| ODP | Ozone Depleting Potential | λ | Fuel Equivalence Ratio |
| ORC | Organic Rankine cycle | η | efficiency/effectiveness |
| ICE | Internal combustion engine | | |
| IHX | Internal heat exchanger | **Subscripts** | |
| UA | Heat exchanger overall thermal conductance | 1,2,...15 | State 1,2,...15 |
| A | Heat exchanger surface area | i, inlet | inlet state |
| U | Overall heat transfer coefficient | e, exit | exit state |
| ECHA | European Chemical Agency | B | Brayton |
| A/C | Air conditioner | R | Rankine |
| APU | Auxiliary Power Unit | GH | Gas heater |
| EES | Engineering Equation Solver | net | net amount |
| $CO_2$ | Carbon dioxide | comb | combustor |
| $CH_4$ | Methane | reg | regenerator |

## 1.0 Introduction

According to a waste heat recovery report by the U.S. DOE, industrial processes in the United States consume approximately 32 quadrillion BTU (quads) of energy annually (BCS Inc., 2008). This amount totals about one third of total energy consumed in the United States. The report also estimates that 20-50 % of that energy is lost to waste heat (BCS Inc., 2008). The report categorizes the waste heat based on the temperature of the waste product. The three waste heat groups are Low, Medium, and High-temperature. Table 1 defines the temperature range for each source based on a limited sample of industrial applications. Table 1 also shows the amount of waste heat and work potential of each waste heat group (BCS Inc., 2008). The units of heat and work are in quads per year. The waste heat and work potential are based on a reference temperature of 25 ºC. This data indicates that Low-temperature waste heat results in 60 % of total waste heat. It is estimated that 287 trillion BTU per year or 32 % of this Low-temperature waste heat can be recaptured into useful work. Low-temperature waste heat recovery therefore presents the largest opportunity to recover energy from otherwise discarded heat.

### 1.1 Pinch Problem

A common method to convert process waste heat to useful work is through a combined cycle. The bottoming cycle may be a gas power or vapor power system in

| | Temperature Range | | Waste Heat (trillion BTU per year) | | Work Potential (trillion BTU per year) |
|---|---|---|---|---|---|
| | °F | °C | 77F [25°C] *Reference* | 300F [150°C] *Reference* | 77F [25°C] *Reference* |
| Low | < 450 | < 230 | 903 | 37 | 287 |
| Med | 450–1200 | 230-650 | 466 | 130 | 216 |
| High | >1200 | >650 | 108 | 89 | 86 |
| Total | - | - | 1478 | 256 | 589 |

Table 1: Yearly national unrecovered waste heat

which heat is transferred between cycles via a heat exchanger (HX). A popular type of heat exchanger is a heat recovery steam generator (HRSG) which combines an economizer, an evaporator, and a superheater ( Kehlhofer, 1997). Marrero et al. use the steam product of a HRSG to power a bottoming cycle (2002). Utilizing a HRSG, combined power cycles capable of achieving 60 % thermal efficiency have been constructed (Siemens Energy, 2013). In a HRSG the hot exhaust gas heats another working fluid from a liquid to a two phase mixture, a saturated vapor, or a superheated vapor. The exit state depends on the amount of heat added and the mass flow rate of the working fluid in the bottoming cycle(Ganapathy, 2006).

Figure 1(a) shows an example of the cooling curve in a HRSG (Chen et al., 2006). Heat is supplied to the working fluid as it goes through a phase transition. Notice that the working fluid remains at a constant temperature during phase change. The fluid of the heat source undergoes what is called sensible cooling during which the temperature continuously decreases.

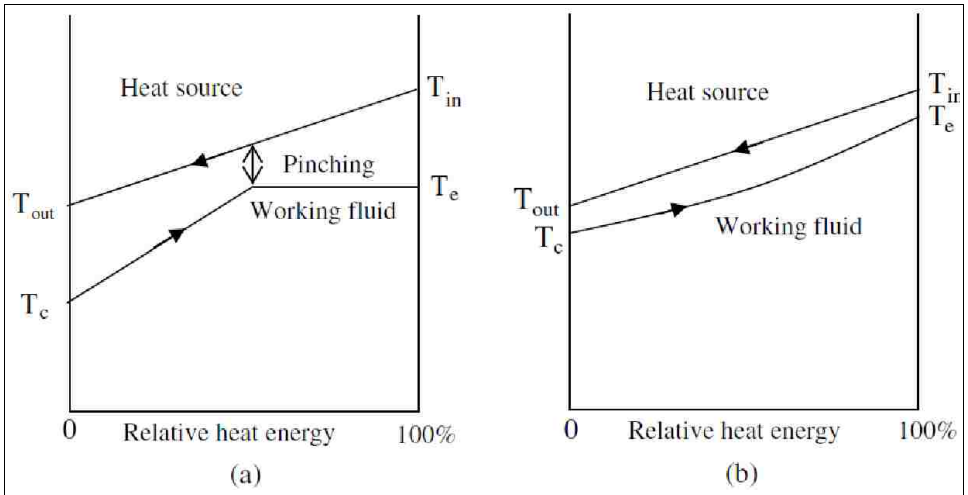

Figure 1: Heating curve in a heat exchanger

Also shown in Figure 1(a) is the pinch point which is the minimum temperature difference between fluids in the heat exchanger. The existence of the pinch point causes

two undesirable effects:

1. The temperature difference at the pinch point reduces the effectiveness of the heat exchanger. Heat transfer between the two fluids is proportional to the temperature difference. As a result, the minimum rate of heat transfer occurs at the pinch point. This reduces the total amount of heat that can be supplied to the working fluid.
2. In order to prevent a reversal of heat transfer direction, the average temperature difference between fluids must be larger than would be necessary with a single phase fluid (refer to Figure 1(a)). These relatively larger temperature differences (temperature gradients) on both sides of the pinch point result in more entropy production within the heat exchanger.

A proposed solution to the pinch problem is to use a single phase working fluid that more closely matches the heat source fluid temperature profile (Chen et al., 2006). This would result in sensible cooling or a "temperature glide" in the heat exchanger. Supercritical fluids remain in a single phase but compared to gases, have smaller specific volumes and better transport properties (Kim et al., 2004). A system using a supercritical working fluid therefore has a relatively low volume to power ratio (Feher, 1968). This low volume to power ratio requires smaller system components to achieve the same power output (Wright, 2012). It is proposed by many authors to use supercritical fluids for application to waste heat recovery (Chen et al., 2006; Persichilli et al., 2012; Cayer et al., 2009; Velez et al., 2011; Chen et al., 2005; Austin and Sumathy, 2011).

Figure 1(b) shows a schematic of the behavior of a supercritical working fluid in a heat exchanger with a sensible heat source. This study will investigate the performance of

a Rankine bottoming cycle using supercritical carbon dioxide for waste heat recovery.

## 1.2 Working Fluid Selection

Table 2 lists critical properties and environmental properties of common refrigerants that can potentially be used as the working fluid. Carbon dioxide has favorable characteristics for the following reasons:

- relatively low critical temperature is well suited for low-temperature heat sources,
- stability and inertness over the temperature range of interest (Chen et al., 2005),
- moderate critical pressure of 73.9 bars,
- abundance, nonflammability and non-toxicity (Cayer et al., 2009),
- well known thermophysical properties in supercritical region (Velez et al., 2011),
- environmentally friendliness with ozone depletion potential (ODP) of 0 and global warming potential of 1 over 100 years (McQuay Air Conditioning, 2002),
- limited research and information available for $CO_2$ power cycle with low temperature heat source (Velez et al., 2011),
- relatively miniaturized system due to a high volumetric heating capacity (Austin and Sumathy, 2011). Due to carbon dioxide's suitability for application in transcritical low-temperature waste heat recovery, it will be the working fluid used in this present analysis.

| Name | Refrigerant Number | Formula | Critical Temperature[a] C(F) | Critical Pressure[a] MPa (psi) | Ozone Depletion Potential[b] | Global Warming Potential[b] |
|---|---|---|---|---|---|---|
| Ammonia | R-717 | $NH_3$ | 133 (270) | 11.2 (1636) | 0 | 0 |
| Carbon Dioxide | R-744 | $CO_2$ | 31 (88) | 7.4 (1072) | 0 | 1 |
| Water | R-718 | $H_2O$ | 374 (705) | 22.1 (3205) | 0 | <1 |
| Propane | R-290 | $CH_3CH_2CH_3$ | 97 (206) | 4.3 (619) | 0 | ~0 |
| Butane | R-600a | $CH_3CH_2CH_2CH_3$ | 152 (305) | 3.8 (551) | 0 | ~0 |
|  | R-22 | $CHCIF_2$ | 96 (205) | 5 (722) | 0.055 | 1500 |

Table 2: Critical and environmental properties of common refrigerants.

## 2.0 Literature Review

According to many papers, studies on the behavior of carbon dioxide in low-temperature transcritical power cycles are not extensively reported(Chen et al., 2006; Cayer et al., 2009; Velez et al., 2011). To better understand the behavior of these types of systems, more research is required. In the interest of waste heat recovery, some researchers analyze various configurations of $CO_2$ bottoming cycles or organic Rankine bottoming cycles. Other researchers directly compare carbon dioxide power cycles to organic Rankine cycles (ORC). Some of the sources of heat in these papers include solar, combustion exhaust gasses, and other generalized industrial waste heat sources. A second law analysis of $CO_2$ bottoming cycle with variations in topping cycle parameters has not been exhaustively reported. Therefore, the necessity for a second law analysis of the "full system" behavior is a major motivation for this study.

### 2.1 Organic Rankine Cycles

Roy et al. conduct a theoretical analysis of bottoming ORC operating with R12, R134a, and R123 as the working fluid (2010). The goal of the study is to determine which of the three working fluids investigated is best suited for application to waste heat recovery. The selection of each organic working fluid is based on the slope of the saturated vapor curve for each. The vertically sloped or "isentropic fluid" is R12. The positively sloped or "dry fluid" is R123. The negatively sloped or "wet fluid" is R123a. The naming convention is due to the turbine exit state: a superheated gas with a "dry fluid", a saturated vapor with an "isentropic fluid", and a liquid-vapor with a "wet fluid". An example of a "wet fluid" is shown in Figure 11. The waste heat is based on data from the NTPC Kahalgaon plant. Exhaust gas at 140 °C and 312 kg/s is used to heat the

bottoming cycle. The bottoming cycle in the analysis consists of a HRSG, a turbine, a condenser, and a pump. The system energetic efficiency, exergetic efficiency, and work output are maximized for each working fluid by varying the turbine inlet pressure in the ORC. A summary of the results is given in Table 3. In the application of waste heat power generation, maximum power production is the primary design criteria. Of the three working fluids, R123 has the highest power production. The author concludes that the gradient of the saturated vapor line on a temperature versus entropy plot affects the efficiency of the system. Also, the lower pinch point temperature in the R123 cycle results in the highest exergetic efficiency (Roy et al., 2010).

Velez et al. compare the maximum efficiency of an ORC using common refrigerants with a maximum source temperature of 150 °C (2012). The organic fluids in the study are R134a, R152, R290, R718, R600, and R600a. The analysis is performed by the process simulator HYSYS®. The authors use the energetic efficiency to evaluate the working fluids' performance in the cycle. The input parameters are the turbine inlet temperature and the pressure ratio of the cycle. The results indicate that for the "wet fluids" R152a, R290, and R718, the energetic efficiency increases with an increase in turbine inlet temperature. For the "dry fluids" R600 and R600a, the energetic efficiency decreases with an increase in turbine inlet temperature. For the "isentropic fluid" R134a,

| Parameters/outputs | Working Fluid | | |
|---|---|---|---|
| | R-12 | R-123 | R-134a |
| Power generated (MW) | 9.13 | 19.09 | 11.71 |
| First law efficiency (%) | 12.09 | 25.30 | 15.53 |
| Second law efficiency (%) | 30.01 | 64.40 | 37.80 |
| Mass flow rate (kg/s) | 541.8 | 341.2 | 417.8 |
| Condenser water flow rate (kg/s) | 1980 | 1712 | 1899 |
| Pinch point (°C) | 19.00 | 5.00 | 25.00 |

Table 3: Summary of results from Roy et al. (2010)

the energetic efficiency is unaffected by variation in turbine inlet temperature. In every case, the energetic efficiency increases with an increase in cycle pressure ratio. In a direct comparison of the six organic fluids tested, R152 achieves the highest energetic efficiency.

Vaja et al. investigate a combined cycle with an internal combustion engine (ICE) as the topping cycle with a bottoming ORC (2010). The two heat sources in the study for the bottoming cycle are the engine coolant and the exhaust gas. Three configurations of the ORC are analyzed. Figure 2 shows a schematic representation of the three setups.

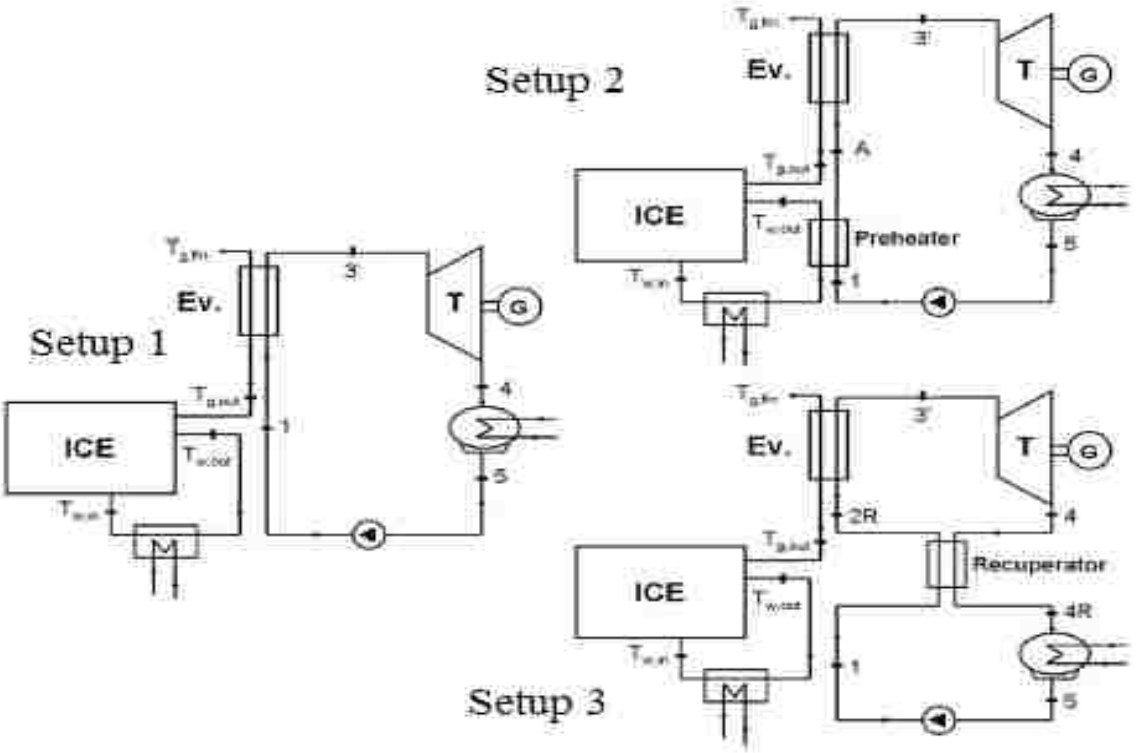

Figure 2: Schematic of setups used by Vaja et. al. (2010)

In all cases the bottoming cycle contains a turbine, a condenser, and a pump. The differences between the three setups are the following:

- *Setup 1*: A simple Rankine cycle heated by the ICE exhaust gas.
- *Setup 2*: The same as *Setup 1* with an included Rankine cycle preheater attached

to the ICE coolant.

- *Setup 3*: The same as *Setup 1* with an included IHX in the Rankine cycle.

Each configuration is analyzed with R11, R134a, and benzene as the bottoming cycle working fluid. Therefore, a total of nine unique systems are analyzed. The analysis assumes exhaust gas at 470 °C with a flow rate of 4.35 kg/s and engine coolant at 90 °C at a flow rate of 24 kg/s. Table 4 shows the combined cycle energetic efficiency for each setup with each respective working fluid. The top portion shows the combined cycle efficiency while the bottom portion shows the relative improvement over the baseline efficiency of the internal combustion engine alone. The efficiency of the standalone internal combustion engine is estimated to be 41.8 %.

Vaja et al. analyze the regenerated cycle only with benzene because benzene is the only "dry fluid" of the three being investigated (2010). Furthermore, these "dry fluids" are the type most commonly used in commerce. Benzene achieves the highest 1st Law efficiency for *Setup 1* and *Setup 2*. The analysis also reveals that utilizing preheat or regeneration (at least with benzene) is more efficient than a simple Rankine bottoming cycle alone.

| **Combined Cycle Efficiency** | | | |
|---|---|---|---|
| | Simple cycle | Simple cycle with preheat | Regenerated cycle |
| Benzene | 46.6% | 47.1% | 47.1% |
| R-11 | 45.8% | 46.3% | - |
| R-134a | 43.8% | 44.5% | - |
| | | | |
| **Relative Improvement over Baseline** | | | |
| Benzene | 11.4% | 12.6% | 12.8% |
| R-11 | 9.5% | 10.8% | - |
| R-134a | 4.8% | 6.5% | - |

Table 4: Cycle efficiencies obtained by Vaja et al. (2010)

## 2.2 Comparison of $CO_2$ to Other Working Fluids

Guo et al. present a theoretical analysis of natural and conventional working fluids in a regenerated Rankine cycle with a geothermal heat source (2010). The temperature range of the heat source is 80-120°C. To define a reference temperature for heat addition and rejection in the heat exchangers, the thermodynamic mean temperatures are implemented and are defined as:

$$\overline{T}_{add} = \frac{h_e - h_i}{s_e - s_i} \quad , \tag{1}$$

for heat addition and

$$\overline{T}_{reject} = \frac{h_i - h_e}{s_i - s_e} \quad , \tag{2}$$

for heat rejection where "h" is the state enthalpy and "s" is the state entropy with the "i" subscript indicating the device inlet state and the "e" subscript indicating the device exit state. $CO_2$ is the baseline for comparison to the other fluids. A pinch-point temperature difference of 5 °C is chosen. Guo et al. observe that the pinch point in the gas heater for transcritical $CO_2$ occurs at the outlet state, i.e. the turbine inlet state (2010).

Table 5 shows a comparison of the results obtained by Guo et al. for each working fluid tested with a thermal source temperature of 100 °C (2010). R115 achieves the highest thermal efficiency. R218 generates the highest net power which is likely due to having

| Fluid | Heat source H/X exit temperature (°C) | Thermal Efficiency (%) | Net power (kW) | UA (kW/K) | Volumetric expansion ratio | Pressure ratio |
|---|---|---|---|---|---|---|
| $CO_2$ | 45.7 | 6.45 | 1.38 | 5.87 | 1.62 | 1.84 |
| R-115 | 63.2 | 9.37 | 1.37 | 3.90 | 4.63 | 3.52 |
| R-41 | 42.5 | 6.99 | 1.59 | 6.90 | 1.92 | 2.16 |
| R-218 | 41.8 | 7.48 | 1.73 | 7.57 | 8.25 | 4.41 |
| R-170 | 49.9 | 6.99 | 1.38 | 5.98 | 1.87 | 1.93 |

Table 5: Summary of results from by Guo et al. (2010)

the highest pressure ratio and volumetric expansion ratio. R218 also has the highest heat exchanger overall thermal conductance (UA), resulting in the lowest heat source temperature of 41.8°C.

In regard to the pinch problem, Chen et al. compare an ORC using R123 to transcritical $CO_2$ power cycle (2006). A regenerated Rankine cycle is used for both cycles with a minor difference being the transcritical cycle contains a gas heater and the ORC contains an evaporator. The authors speculate that for a cycle using waste heat at moderate temperature (80-200 °C) as a heat source, the best efficiency and highest power output is obtained when the working fluid temperature profile can match the temperature profile of the heat source (Y. Chen et al., 2006). The authors use the thermodynamic mean temperature for heat transfer in the heat exchangers. The analysis is performed with EES (Klein, 2006). A comparison of the results for the transcritical $CO_2$ power cycle and the R123 ORC are provided in Table 6. The $CO_2$ has a turbine inlet temperature of 140 °C which is more than 55 °C above the turbine inlet temperature using R123. In addition, the exhaust gas temperature leaving the HX is 12.7 °C lower when using R123. This indicates that more heat is indeed extracted from the exhaust gas. The premise that transcritical $CO_2$ would more effectively capture heat from the exhaust gas appears to be confirmed. The only apparent drawback to using transcritical $CO_2$ is that a smaller expansion ratio must be used because of the relatively high condenser pressure required. Even with a smaller expansion ratio, the carbon dioxide cycle was able to achieve about a 1.2 % increase in power output versus R123.

| Working Fluid | Turbine inlet temperature(°C) | Heat addition pressure(bar) | Exhaust gas exit Temperature(°C) | Specific power output(kW/kg) | Expansion Ratio |
|---|---|---|---|---|---|
| $CO_2$ | 140 | 16 | 61.3 | 8.16 | 2.67 |
| R123 | 84.4 | 5.3 | 74 | 8.06 | 6.91 |

Table 6: Summary of results from Chen et al. (2006)

Cayer et al. compares ethane, R125, and $CO_2$ in transcritical power cycles (2010). A simple Rankine cycle is analyzed with a heat source being an industrial gas at a temperature of 100 °C with a mass flow rate of 314.5 kg/s. The system input parameters are the turbine inlet temperature and the turbine inlet pressure. The analysis is conducted in four sections. The first two sections are an energy and exergy analysis, respectively. The third section is a finite size thermodynamic analysis which determines UA. The fourth and final section of the analysis determines the required surface area of each heat exchanger by using empirical approximations for the overall heat transfer coefficient, "U". Figure 3 shows the 1st Law efficiency and specific net work, with $CO_2$ as the working fluid, plotted versus turbine inlet pressure (shown as maximum pressure) and the turbine inlet temperature (shown as $T_{max}$). As the turbine inlet temperature increases, both the thermal efficiency and the net specific work increase. It should be noted that as the turbine inlet temperature approaches the temperature of the thermal source (100 °C), the required heat exchanger surface area becomes impossibly large.

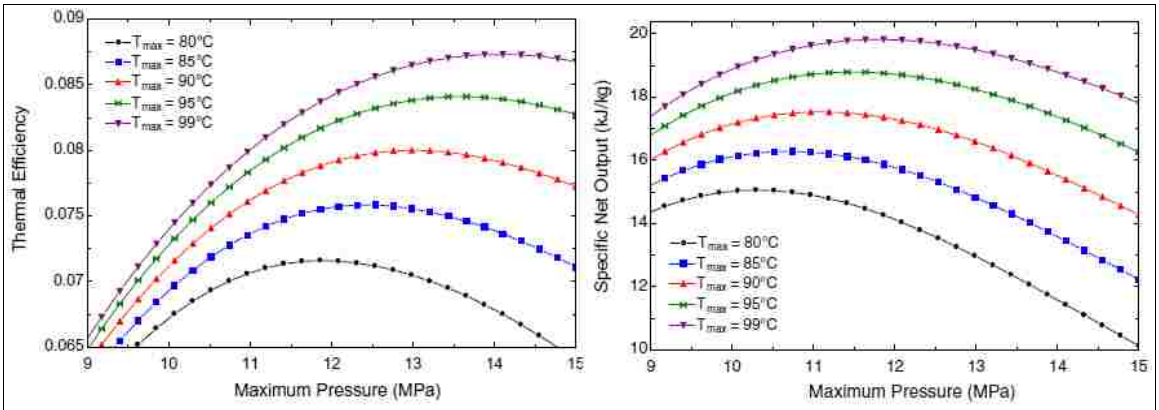

Figure 3: 1st Law efficiency and net specific work versus turbine inlet temperature from Cayer et al. (2010)

It can be concluded from the figure that it is impossible to maximize both the thermal efficiency and the net specific work simultaneously. Cayer et al. conclude that in

application to waste heat recovery, focus should be on maximizing the net specific work rather than the thermal efficiency (2010).

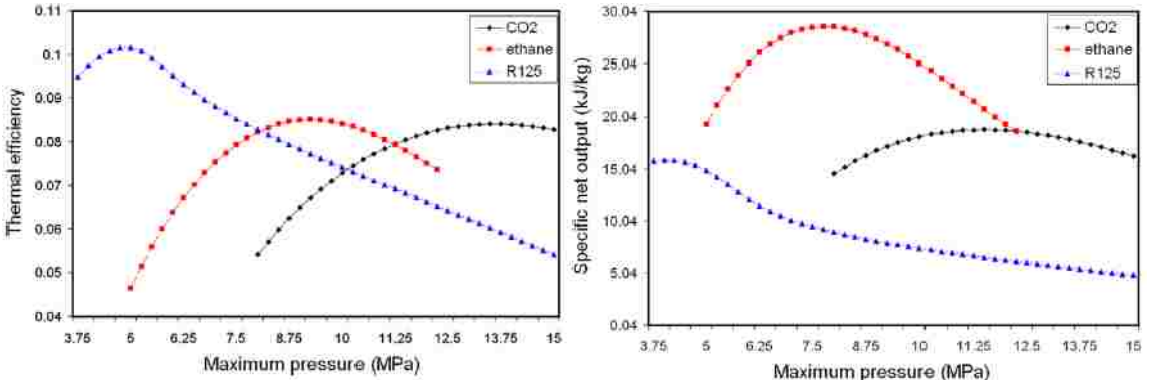

Figure 4: Thermal efficiency and net specific work versus fluid and TIP from Cayer et al. (2010)

Figure 4 compares the thermal efficiencies and net specific works for all three working fluids evaluated versus turbine inlet pressure. R125 has the highest thermal efficiency of about 10 %. Ethane has the highest net specific work of about 29 kJ/kg. Although ethane has the highest net specific work, it is flammable and requires the largest "A" of the fluids sampled (Cayer et al., 2010).

Chen et al. compare R32 to $CO_2$ in a transcritical Rankine cycle utilizing low grade heat at temperatures ranging from 373-453 K (100-180 °C) . An energetic and

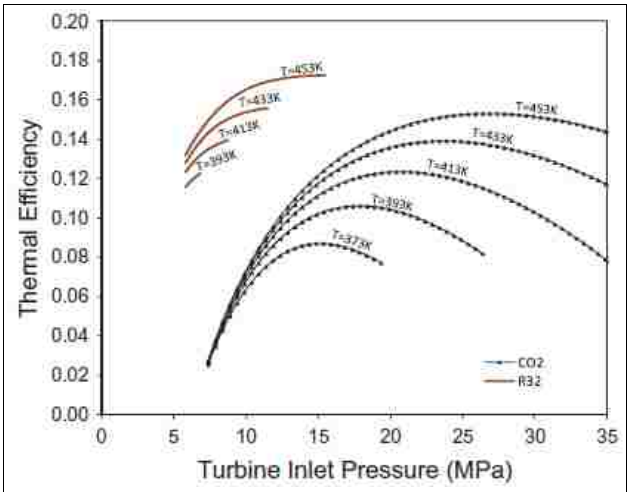

Figure 5: Thermal efficiency results from Chen et al.(2010)

exergetic analysis is performed. Figure 5 compares the thermal efficiencies of $CO_2$ and R32 at various turbine inlet temperatures and turbine inlet pressures. It is apparent that transcritical R32 achieves higher thermal efficiencies than transcritical $CO_2$ and at lower operating pressures. Despite the higher thermal efficiencies, R32 is rated "highly flammable" by the ECHA classification system. The high flammability of R32 prevents its use in applications where safety is the primary concern. The exergy distribution and 2nd Law efficiency for $CO_2$ is shown in Figure 6. The turbine inlet temperature is held constant at 433 K. The greatest source of exergy destruction within the cycle is the condenser. For a given turbine inlet temperature, the maximum exergetic efficiency and maximum net power occur at different pressures at the turbine inlet.

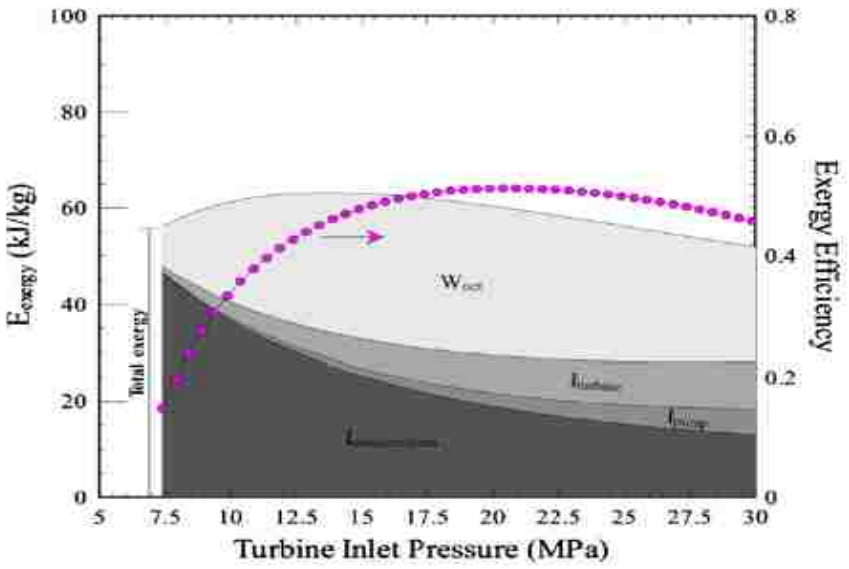

Figure 6: Exergy results from Chen et al. (2010)

### 2.3 Bottoming Cycles with $CO_2$

Persichilli et al. describe a waste heat recovery power system developed by Echogen Power Systems LLC (2012). The cycle is a recuperated Rankine cycle with supercritical $CO_2$ as the working fluid. The system is designed to use industrial process

waste heat between 200 °C (473 K) and 540°C (813K). The system is scalable to produce 250-50,000 kW. A noted advantage of a supercritical system over a traditional ORC is the component miniaturization. A size comparison between the Echogen 10 MWe supercritical $CO_2$ turbine and an equivalent steam turbine is shown in Figure 7 (Persichilli et al., 2012).

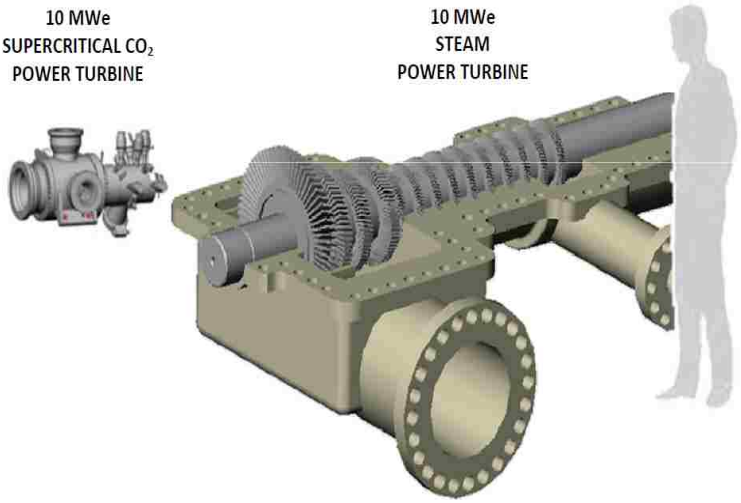


Figure 7: Supercritical $CO_2$ turbine and steam turbine size comparison

The authors also mention another advantage of using a supercritical working fluid instead of a subcritical working fluids is pinch point avoidance. Persichilli et al. predict that the system can reduce the Levelized Cost of Electricity by 10-20 % with efficiencies up to 30 % (2012).

F. Velez et. al. conduct an analysis on a transcritical $CO_2$ power cycle with a low temperature heat source (2011). An energy and exergy analysis, performed in HYSYS®,

| | Parameter | | | | |
|---|---|---|---|---|---|
| | TIT (°C) | TIP (bar) | Energetic Efficiency (%) | Exergetic Efficiency (%) | Net Specific Work (kJ/kg) |
| with IHX [without IHX] | 150 | 141.0 [161.0] | 9.8 [8.0] | 48 [38] | 18.1 [18.0] |
| | 120 | 124.0 [136.5] | 7.3 [6.4] | 46 [36] | 12.6 [12.5] |
| | 90 | 106.0 [114.0] | 4.8 [4.5] | 43 [34] | 7.7 [7.6] |
| | 60 | 88.5 [92.5] | 2.4 [2.5] | 40 [30] | 3.5 [3.4] |

Table 7: Summary of results from Velez et al. (2011)

is conducted on a simple Rankine cycle and on a regenerated Rankine cycle. The input parameters are the turbine inlet temperature and the turbine inlet pressure.

Table 7 shows the results obtained when the net specific work is maximized by varying the turbine inlet pressure for each selected temperature at the turbine inlet. The obvious benefit of increasing the turbine inlet temperature is an increase of the net specific work. The table also indicates that as the turbine inlet temperature increases, the pressure at the turbine inlet must increase to achieve the maximum net specific work (Velez et al., 2011).

Similarly to the behavior observed by Cayer et al. (2010), the authors notice there is no operation point that simultaneously produces maximum efficiency and maximum net specific work. In all cases analyzed, inclusion of an IHX increased the exergetic efficiency but had little effect on the net specific work.

To reduce fuel consumption in automotive applications, Chen et al. proposes three system layouts to utilize ICE exhaust gas waste heat (2005). The first design concept, named the Reversible Cycle, is illustrated in Figure 8(a). It is a redesign of the existing A/C cycle which can run in reverse as a transcritical power cycle when compartment

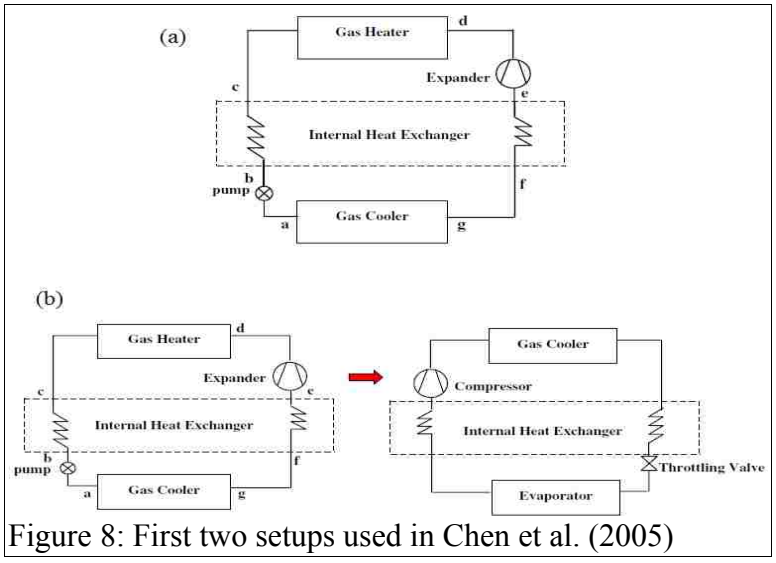

Figure 8: First two setups used in Chen et al. (2005)

cooling is not necessary. The gas heater pressure is set to 130 bar and the gas cooler pressure is set to 60 bar. The turbine inlet temperature is preset to 200 °C. Figure 8(b) shows the second cycle design concept which contains the existing A/C system with an added parallel power cycle. This setup, named the Auxiliary Power Unit (APU), can be used to produce electricity and heat when the ICE is idling or function as a Brayton cycle to convert waste heat into extra power. The heat source is the ICE exhaust gas. The APU is analyzed for two different operating scenarios. The first scenario operates as a transcritical cycle with the gas heater pressure set to 300 bar and the condenser pressure is set to 60 bar. The second scenario operates entirely in the supercritical region as a Brayton cycle with the gas heater pressure maintained at 300 bar and the gas cooler pressure raised to 100 bar. The turbine inlet temperature is increased to 350 °C. The third design concept layout, named the Combined Cycle, is illustrated in Figure 9. Internal heat exchangers are included in all setups with the intention of improving efficiencies.

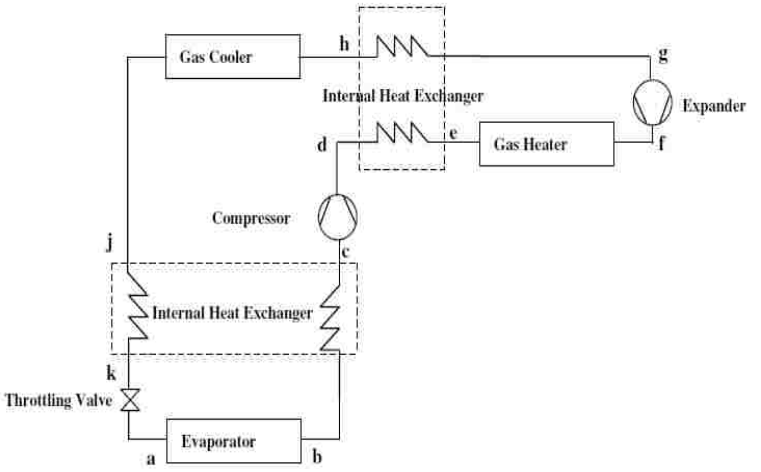

Figure 9: Combined cycle layout from Chen et al. (2005).

A summary of system parameters and results is provided in Table 8. For each setup, the thermal efficiency is calculated using an internal heat exchanger effectiveness of 60 % and 90 %. Note that the second heat addition pressure for the combined cycle

represents the evaporator pressure. The table indicates the highest thermal efficiency is achieved by the reversible cycle with an internal heat exchanger effectiveness of 90 %. The configuration with the lowest thermal efficiency is the combined cycle with a recuperator effectiveness of 60%. Although the supercritical APU cycle appears to have a higher efficiency than the transcritical version, it should be noted that the pressure ratios and turbine inlet temperatures of the two cycles differ. The authors determine that even by varying the internal heat exchanger effectiveness, the Reversible Cycle always has the highest thermal efficiency (Chen et al., 2005).

Cayer et al. analyze two transcritical $CO_2$ bottoming cycles for low temperature heat addition (2009). The first is a simple Rankine cycle and the other is a simple Rankine cycle with an internal heat exchanger. The analysis procedure is the same used by Cayer et al. (2010). The input parameters are α and the turbine inlet temperature. The term "α" is the percentage power output compared to power output at Carnot efficiency. The turbine inlet pressures that maximize the thermal efficiency and those that maximize the exergetic efficiency for each of the two setups with assumed values of α are presented in Table 9. For example, for a cycle without an IHX and at α = 0.20, the maximum exergetic efficiency is 58.1 % and occurs at a turbine inlet pressure of 13.5 MPa. Cayer et al. observe that α does not have an influence on the specific net power output or the thermal efficiency (2009). Also, at a turbine inlet pressure above 12.8 MPa, an internal

| Setup Name | Input Parameters | | | Results | |
|---|---|---|---|---|---|
| | Heat addition Pressure (bar) | Heat rejection pressure (bar) | TIT (°C) | Thermal efficiency IHX η= 60% | Thermal efficiency IHX η= 90% |
| Reversible Cycle | 130 | 60 | 200 | 0.19 | 0.31 |
| APU Transcritical Cycle | 300 | 60 | 200 | 0.12 | 0.13 |
| APU Supercritical Cycle | 300 | 100 | 350 | 0.15 | 0.20 |
| Combined Cycle | 150/40* | 100 | 350 | 0.05 | 0.14 |

Table 8: Summary of input parameters and resulting thermal efficiencies for each setup

heat exchanger cannot be used because the temperature at the turbine exit is lower than the temperature at the pump outlet. Therefore, the internal heat exchanger is counterproductive above 12.8 MPa. Table 9 also indicates that the cycle exergetic efficiency varies with α and turbine inlet pressure. Despite this result, the authors observe that the "relative" exergy destruction within each component is not dependent on the values of α and high pressure (Cayer et al., 2009). The obtained values of relative exergy destruction within each component are, 50% in the vapor generator, 27% in the turbine, 11% in the condenser, 7% in the pump and less than 5% in the recuperator.

In consideration of the component-wise exergy destruction, the authors conclude that effort should be made on improving the temperature matching between the heat source and the working fluid in the evaporator (Cayer et al., 2009).

Chacartegui et al. analyzes a $CO_2$ power cycle operating entirely in the supercritical regime (Chacartegui et al., 2011). Heat is introduced through a solar collector. A bottoming ORC is added to recover waste heat from the cycle. The pressure ranges from 7.5 MPa to 22.5 MPa, resulting in a pressure ratio of 3.0. With a turbine inlet temperature of 1100 K, the energetic efficiency of the topping cycle is found to be about 38% (Chacartegui et al., 2011). By reducing the pressure in the gas cooler, a larger

**Cycle without IHX**

| α | Max Thermal Efficiency (%) | Turbine inlet temperature (MPa) | Max Exergetic Efficiency (%) | Turbine inlet temperature (MPa) |
|---|---|---|---|---|
| 0.15 | 8.4 | 13.6 | 63.4 | 13.5 |
| 0.2 | 8.4 | 13.6 | 58.1 | 13.5 |

**Cycle with IHX**

| α | Max Thermal Efficiency (%) | Turbine inlet temperature (MPa) | Max Exergetic Efficiency (%) | Turbine inlet temperature (MPa) |
|---|---|---|---|---|
| 0.15 | 8.6 | 11.3 | 64.6 | 11.3 |
| 0.2 | 8.6 | 11.3 | 59.4 | 11.3 |

Table 9: Summary of results from Cayer et al. (2009)

pressure ratio can be achieved. This larger pressure ratio may result in a larger power output.

# 3.0 Purpose and Methodology

## 3.1 System Description

The system analyzed is a combined power cycle which consists of an air Brayton topping cycle and a transcritical $CO_2$ Rankine bottoming cycle. Assumptions for the system are the following:

1. All processes happen in quasi-equilibrium steps and occur at steady state.
2. An air-standard cycle analysis is used for the topping cycle (this assumption is explained in greater detail and validated in Section 4.1).
3. The effects of mass change in combustor are negligible (see Section 4.1).
4. All kinetic and potential energy changes are negligible.
5. No pressure or heat losses occur in component connecting tubes.
6. All heat exchangers are well insulated.
7. Irreversibility due to friction within heat exchangers is approximated as parametric pressure drops within each respective stream.
8. The definition of "isentropic efficiency" is used to determine exit states of expansion and compression processes.
9. The definition of "recuperator effectiveness" is a control parameter for the recuperator and internal heat exchanger.
10. Heat addition within the combustor is treated as heat addition from a high temperature thermal reservoir (a reservoir temperature is selected such that exergy destruction is comparable to actual measured values).
11. Carbon dioxide departs the condenser as saturated liquid.
12. Pinch point occurs at a side of the heat exchanger rather than the center due to the

temperature glide condition shown in Figure 1(b).

13. Internal geometry of the heat exchanger are such that the parametric temperature differences between inlets and outlets are possible.

A schematic of the system layout is presented in Figure 10. Each component is labeled along with associated intermediate states. Air enters the compressor at ambient conditions. Air leaves the compressor at state 2 and enters the cold steam side of the recuperator where it is preheated by exhaust gas. The air next leaves the recuperator at state 3 and enters the combustor. Within the combustor, heat is supplied from the combustion of air with methane. Exhaust gas leaves the combustor at state 4 and expands through Turbine 1. Exiting Turbine 1, the expanded exhaust gas enters the hot stream side

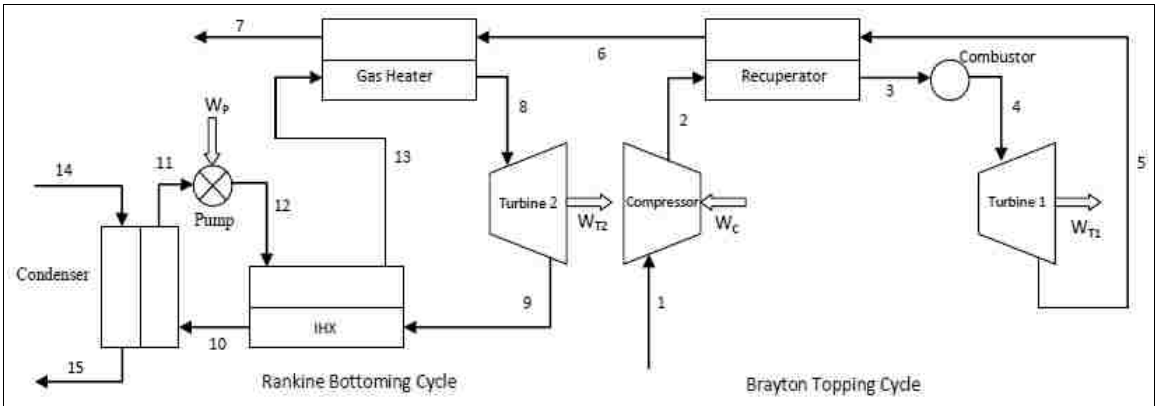

Figure 10: Combined cycle layout

of the recuperator at state 5. The high enthalpy exhaust gas leaves the hot stream side of the recuperator and proceeds into the hot stream side of the gas heater. Within the gas heater, heat is transferred from the Brayton cycle exhaust gas to the carbon dioxide in the Rankine cycle. The low enthalpy exhaust gas at state 7 is then discharged into the environment.

Supercritical $CO_2$ at state 8 enters Turbine 2 where it is expanded. Between states 9 and 10, heat is rejected to the cold stream side of the IHX. The $CO_2$ at state 10 then

enters the condenser where it exits as saturated liquid at state 11. Next, the $CO_2$ passes through the pump followed by the cold stream side of the IHX. Finally, $CO_2$ exits the IHX at state 13 where it enters the Rankine side of gas heater and the cycle is repeated. Water enters the condenser at ambient temperature. If at some point during operation, the inlet temperature of the cooling water exceeds the 31°C critical temperature of $CO_2$, the cycle would operate entirely in the supercritical regime.

An alternative cycle layout removes the IHX and instead uses the condenser to produce domestic hot water at state 15. For simple adaptation of the EES program in APPENDIX B, state 10 would equal state 9 and state 13 would equal 12. The domestic hot water must exit at 149 °F (65 °C). Holding the domestic hot water at a constant temperature, variation of the temperature at state 9 would cause an appropriate variation of the domestic hot water flow rate.

A temperature versus entropy diagram of the bottoming $CO_2$ cycle is shown in Figure 11. The figure shows actual states and applicable isentropic states. For example, state 9s designates where state 9 would be if expansion within Turbine 2 was isentropic.

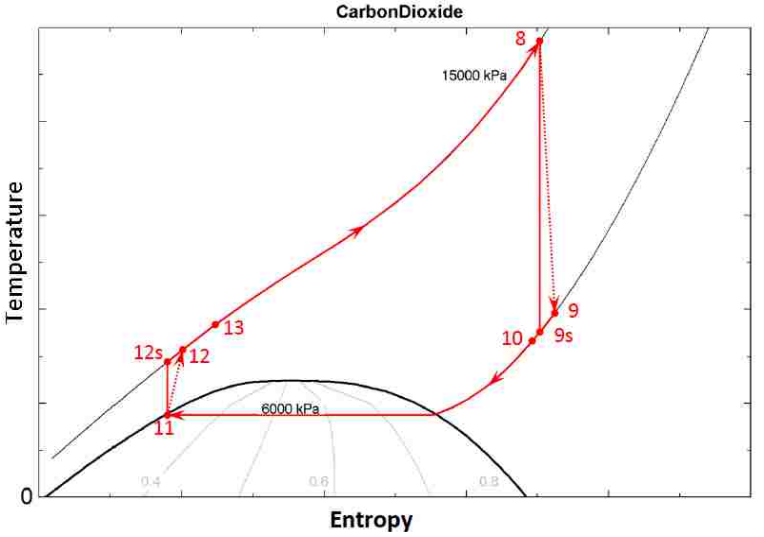


Figure 11: Temperature versus entropy plot of transcritical $CO_2$ Rankine cycle

It should be noted that pressure losses within the heat exchangers are not depicted in the figure but will be included in the analysis. Also, the pressures shown may not be the nominal values used in the analysis.

## 3.2 Purpose Statement

The purpose of this study is to quantify the performance of the transcritical bottoming cycle and to quantify the performance of the combined cycle as a whole by altering system parameters to gain insight for future research and development efforts in the field of waste heat recovery. The performance of the system will be quantified through common effectiveness measurements of energy utilization. These measurements will include energetic efficiencies, exergetic efficiencies, and component-wise irreversibilities.

## 3.3 Methodology of Analysis

A First Law and Second Law of Thermodynamics analysis will be conducted on the system using EES (Klein, 2006). The thermodynamic properties for air are taken from the EES definition "Air" which is approximated as an ideal gas. Thermodynamic properties for $CO_2$ are taken from the EES definition "CarbonDioxide" which is valid for temperatures up to 1100 K and pressures up to 800 MPa. For "CarbonDioxide", the reference states for enthalpy and entropy are 298.15 K and 101.325 kPa (Klein, 2006). The system has multiple control parameters.

### 3.3.1 System Control Parameters

Table 10 contains a list of system control parameters with associated minimum, maximum, and nominal values. This section explains the rational for selecting the ranges of values.

The minimum and maximum values of ambient temperatures are taken from 5°C (41°F) to 30°C (86°F) which are comparable to most regions of the U.S. throughout the year.

The turbine inlet temperature is limited by current material restrictions. The maximum value for the turbine inlet temperature is due to material limitations. Kehlhofer provides a temperature limit of about 1525 K for commonly available gas turbines (1997).

| Input Parameters | Unit | Value | | |
|---|---|---|---|---|
| | | Minimum | Maximum | Nominal |
| Ambient/Reference Temperature | K | 278 | 302 | 298 |
| Brayton Turbine Inlet Temperature | K | 1200 | 1500 | 1500 |
| Rankine Turbine Inlet Pressure | kPa | 10,000 | 20,000 | 15,000 |
| Brayton cycle Pressure Ratio | - | 3 | 19 | 15 |
| Recuperator/IHX Effectiveness | % | 60 | 1 | 0.8 |
| Brayton Compressor isentropic efficiency | % | 75 | 100 | 85 |
| Rankine Pump isentropic efficiency | % | 75 | 100 | 90 |
| Brayton Turbine (1) isentropic efficiency | % | 70 | 100 | 85 |
| Rankine Turbine (2) isentropic efficiency | % | 70 | 100 | 85 |
| Gas Heater hot end Temperature Difference | K | 5 | 15 | 10 |
| Gas Heater cold end Temperature Difference | K | 2 | 10 | 5 |
| Condenser Approach Temperature Difference | K | 2 | 10 | 2 |
| Recuperator Relative Pressure Loss | % | 0 | 5 | 3 |
| Combustor Relative Pressure Loss | % | 0 | 5 | 3 |
| Gas Heater Relative Pressure Loss | % | 0 | 5 | 3 |
| Condenser Relative Pressure Loss | % | 0 | 5 | 3 |

Table 10: System input parameters

The maximum Brayton cycle pressure ratio is taken from the following equation for maximum work,

$$(P_r)_{max} = \left(\frac{T_{max}}{T_{ref}}\right)^{\frac{k}{[2(k-1)]}} = \left(\frac{1500}{278}\right)^{\frac{1.4}{0.8}} \approx 19 \quad , \tag{3}$$

where $T_{max}$ is the maximum turbine inlet temperature (absolute), $T_{ref}$ is the ambient temperature (absolute), and k is the specific heat ratio for air (Moran and Shapiro, 2008). It should be noted that Brayton cycles operating at relatively high pressure ratios usually include: intercooling between multiple compressor stages to reduce pump work and reheat between multiple expansion stages to increase turbine work (Moran and Shapiro, 2008).

The ranges for the recuperator effectiveness, internal heat exchanger effectiveness, isentropic compressor efficiency and isentropic turbine efficiency are all from Moran and Shapiro (2008). The nominal value for the pump isentropic efficiency is assumed to be slightly higher than for a compressor due to less fluid compressibility in the pump.

For the gas heater, temperature differences between component inlets and exits are used as control parameters rather than the pinch point. Assumption 12 explains why the end temperature difference may be used. The range for the temperature differences is the same used by Chen et al. (2006). Because the condenser exit state is assumed to be saturated liquid, a temperature difference between state 14 and state 11 is used. This temperature difference is required because like the gas heater, a value of zero would require an infinite heat exchanger surface area. The values for the condenser temperature difference are chosen similarly to the gas heater temperature differences (Chen et al., 2006).

### 3.3.2 Evaluation Metrics

Some common thermodynamic metrics are utilized to evaluate and compare the system operating under different parametric conditions. These "figures of merit" include the system 1st Law efficiency, the system 2nd Law efficiency, and component-wise exergy destruction. The 1st Law efficiency is simply defined as,

$$\eta_1 = \frac{\dot{W}_{NET}}{\dot{Q}_{\text{in}}} \quad , \tag{4}$$

where $\dot{W}_{\text{NET}}$ is the net power output and $\dot{Q}_{\text{in}}$ is the rate of heat transfer into the system which in this case comes solely from the combustion process. The 2nd Law efficiency is defined as,

$$\eta_2 = \frac{Exergy\,Used}{Exergy\,Supplied} = \frac{\dot{W}_{net}}{\dot{E}_{fuel}} = \frac{\dot{W}_{net}}{\dot{W}_{\text{net}} + \sum_j \dot{E}_D + \sum_k \dot{E}_{flow}} \quad , \tag{5}$$

where "Exergy Used" is the same net power output from Equation 4, $\dot{E}_{fuel}$ is the rate of exergy addition from fuel, $\sum_j \dot{E}_D$ is the sum of exergies destroyed by each component "j", and $\sum_k \dot{E}_{flow}$ is net amount of exergy flowing across the system control volume via streams "k". The equivalent terms for "Exergy Supplied" in Equation 5 are derived from an exergy balance on the entire system. One goal of this study is to quantify and compare exergy destruction within each component of the system. Another system metric to be determined is the minimum isentropic turbine efficiency in the bottoming cycle which results in a positive net power output. In other words, what is the turbine efficiency at which the power supplied to the pump is equal to the power from the turbine.

### 3.3.3 Analysis Procedure

The first section of the analysis validates the use of an air-standard analysis

instead of a more realistic model. The required enthalpy of combustion is evaluated using the air-standard assumptions and is again evaluated using the dry-product mixture assumptions. A relative difference between the results of the two methods is determined.

The second section is a sensitivity analysis of each input parameter. The parameter of interest is evaluated over the range specified in Table 10. All other input variables are set to their respective nominal value during test run. The purpose of this section is to determine which input variables have the strongest influences on the selected figures of merit.

The alternate cycle which produces domestic hot water is evaluated under nominal parametric values. The feasibility and performance of this alternate configuration is discussed in Section 4.0.

### 3.4 Gas Heater Analysis Methods

The rate of heat transfer between streams in the gas heater is defined as

$$\dot{Q}_{GH} = \dot{m}_B [h(T_6) - h(T_7)] \tag{6}$$

for the Brayton stream and

$$\dot{Q}_{GH} = \dot{m}_R [h(T_8) - h(T_{13})] \tag{7}$$

for the Rankine stream. The terms $\dot{m}_B$ and $\dot{m}_R$ are the mass flow rates of the Brayton topping cycle and the Rankine bottoming cycle, respectively. The subscripts correspond to a property at that state number. The temperature at state 8 is determined by

$$T_8 = T_6 - \Delta T_{HOT} \quad . \tag{8}$$

The topping cycle mass flow rate and $\Delta T_{HOT}$ are control parameters. The temperature at state 6 is determined solely from the topping cycle. The temperature at state 13 is found by working stream-wise starting from the condenser. Two methods can

be implemented to solve for the two unknowns, $\dot{m}_R$ and $T_7$. The methods are as follows:

1. Determine $T_7$ by assuming a temperature difference between states 7 and 13. Solve for the Rankine cycle mass flow rate.
2. Assume a Rankine cycle mass flow rate. Solve for the exit temperature at state 7. Verify that the temperature at state 7 is not less than the temperature at state 13 as that would be an impossible condition. If necessary, modify the Rankine cycle mass flow rate until state 7 is a valid temperature.

In regard to an actual system, the Rankine cycle mass flow rate would be independently controlled. Temperatures at states 7 and 8 would depend on this mass flow rate and heat transfer properties of the gas heater. By assuming that the heat transfer properties of the gas heater are such that the prescribed temperature differences occur (assumption 13), a numerical heat transfer analysis is avoided. Therefore, the second method is used in the EES analysis. The temperature at state 7 is determined by,

$$T_7 = T_{13} + \Delta T_{COLD} \tag{9}$$

where $\Delta T_{COLD}$ is the gas heater cold side temperature difference. By constraining all the input and output state temperatures of the gas heater, the Rankine bottoming cycle mass flow rate dynamically adjusts within the program to satisfy the energy balance.

# 4.0 Results and Discussion

## 4.1 Validation of Air-Standard Analysis

In order to simplify the analysis, the combustion process is studied using an air-standard approach. The following assumptions are made for an air-standard analysis:

- The working fluid is air, which behaves as an ideal gas.
- The temperature rise that would result from combustion is accomplished by heat addition from a thermal reservoir. (Moran and Shapiro, 2008)

A more realistic approach than the air-standard analysis is a dry product analysis. The assumptions made for a dry product analysis are the following:

- Air is approximated on a molar basis as 79% nitrogen and 21% oxygen.
- Product and reactant gases are treated as mixtures of ideal gases.
- The nitrogen present in the combustion is inert and is the same temperature as the other product gases.
- Complete combustion of the fuel occurs.
- Natural gas is modeled as methane ($CH_4$).
- The combustion chamber is adiabatic.

To show the simplification will still yield appropriate results, the program in APPENDIX A compares the required heat addition for a dry product analysis to the required heat for an air-standard analysis.

The specific molar heat additions are calculated for turbine exit temperatures ranging from 1000-2000 K. These results are compared in Figure 11. Note that TIT is held constant at 500 K. The results indicate that to achieve the same temperature, the mixture requires 7-8% more heat addition. This underestimated heat addition for the air-

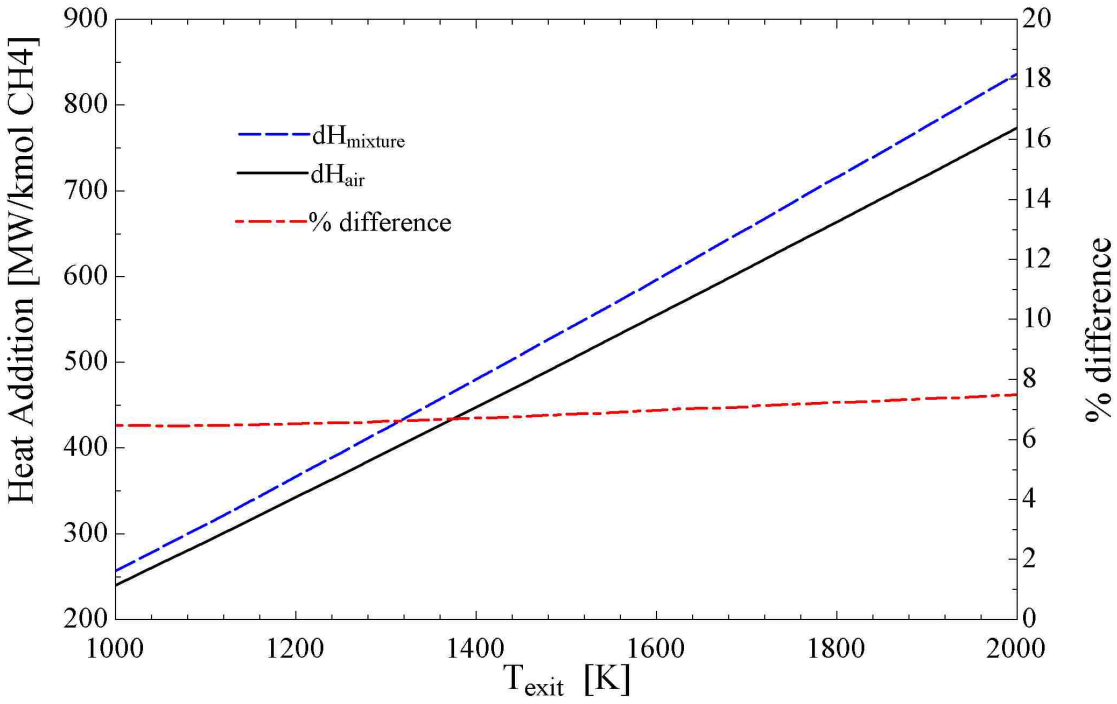

Figure 12: Heat addition versus outlet temperature for ideal air and gas mixture

standard analysis is likely to overestimate the cycle efficiency. What other effects will result from the 8 % difference are unclear. In the interest of computational simplification, the analysis of the topping cycle is conducted using the air-standard approach.

### 4.1.1 Combustion Irreversibility for a Dry Mixture Analysis

Using an air-standard analysis requires a heat reservoir. The temperature of the reservoir must be determined such that the irreversibility within the combustor is comparable to realistic values. The target irreversibility in the combustor is assumed to be 30%. The program in APPENDIX A calculates the irreversibility in the combustor for a dry mixture. The thermal reservoir temperature is assumed to be the adiabatic flame temperature. The analysis is complicated by the fact that irreversibility is a function of both the combustor inlet temperature (which varies by Brayton cycle parameters) and the adiabatic flame temperature (which varies by equivalent fuel ratio, λ). The analysis is

conducted in 2 steps:

1. An "assumed" inlet temperature of 500 K is picked. The adiabatic flame temperature is adjusted via the equivalent fuel ratio until the irreversibility is 30%. From this step, the "target" adiabatic flame temperature is found to be 1620 K. This result forms the "basis" for the next step.
2. For given combustor inlet temperatures, an equivalent fuel ratio is found such that the "basis" adiabatic flame temperature (1620 K) is achieved.

The results of the analysis are provided in Table 11. The results from Step 1 are underlined. The percent irreversibility varies from about 36% at a 300 K combustor inlet temperature to about 23% at a 1000 K inlet temperature. The range of temperatures evaluated is within the expected range of inlet temperatures for the main parametric analysis. The behavior of the irreversibility agrees with common results by which a larger temperature gradient contributes to greater irreversibility.

| $T_{inlet}$ [K] | $T_{flame}$ [K] | Equivalent Fuel Ratio ($\lambda$) | Percent Irreversibilty |
|---|---|---|---|
| 300 | 1618 | 1.75 | 35.80% |
| 350 | 1622 | 1.81 | 34.00% |
| 400 | 1622 | 1.88 | 32.40% |
| 450 | 1621 | 1.96 | 31.10% |
| **500** | **1619** | **2.05** | **30.00%** |
| 550 | 1621 | 2.14 | 28.90% |
| 600 | 1622 | 2.24 | 27.90% |
| 650 | 1620 | 2.36 | 27.10% |
| 700 | 1619 | 2.49 | 26.30% |
| 750 | 1620 | 2.63 | 25.60% |
| 800 | 1621 | 2.79 | 24.90% |
| 850 | 1621 | 2.97 | 24.30% |
| 900 | 1621 | 3.18 | 23.70% |

Table 11: Required fuel equivalence ratio to achieve adiabatic flame temperature of 1620 K for various combustor inlet temperatures.

### 4.1.2 Combustion Irreversibility for an Air-Standard Analysis

The result of the previous analysis yield a reservoir temperature 1620 K. Though the results are interesting, they are not applicable when using the air-standard analysis. The dry mixture analysis inherently accounts for irreversibilities due to the mixing of gasses. To achieve the same amount of irreversibility using an air-standard analysis, a much higher reservoir temperature must be selected. Figure 13 shows the percent exergy destruction in an air-standard combustor versus the reservoir temperature and the combustor inlet temperature. The combustor exit temperature is held constant at 1500 K.

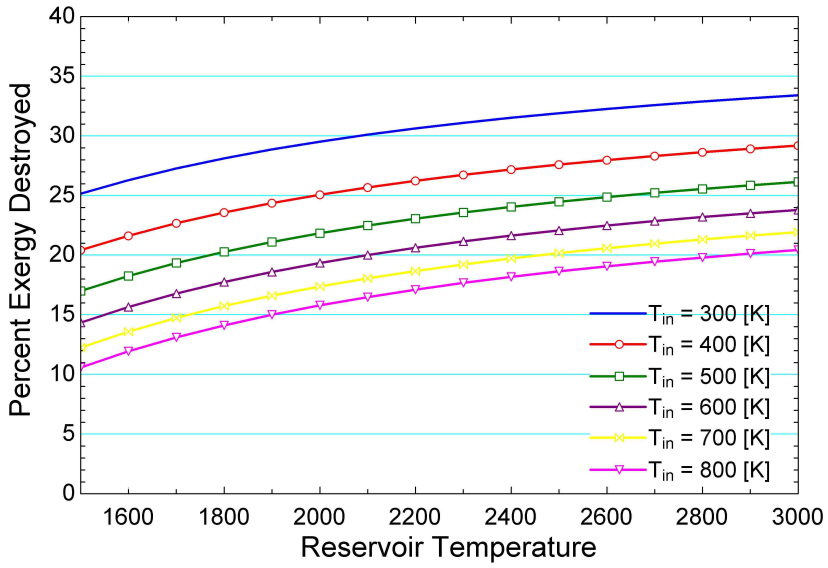


Figure 13: Exergy destruction versus reservoir temperature and combustor inlet temperature

The only inlet temperature shown which approaches 30 % irreversibility is the 300 K combustor inlet curve at a a reservoir temperature of about 2100 K. This condition corresponds to air entering a combustor at the reference temperature. With the introduction of a recuperator, the combustor exergy destruction will surely decline. If the 1620 K reservoir temperature where used the result would be an underestimation in the combustor exergy destruction. Consequently, the exergetic efficiency of the combined

cycle would be overestimated.

## 4.2 Parametric Analysis

The next step of the analysis is the single variation of each parameter in Table 10. Details of the procedure for the analysis are discussed in Section 3.3. Unless otherwise specified, the mass flow rate is constant at 1.0 kg/s.

Variation of the internal heat exchanger effectiveness reveals a critical limitation of the system. An expected result of increasing the internal heat exchanger effectiveness is a corresponding increases in the temperature at state 13. Recall state 13 is the bottoming cycle inlet to the gas heater and state 7 is the topping cycle exit to the gas heater. However, a secondary effect of this increased temperature at state 13 is a reduction in the amount of heat transferred into the bottoming cycle via the gas heater. The excess enthalpy of the exhaust stream is discharged to the environment at state 7.

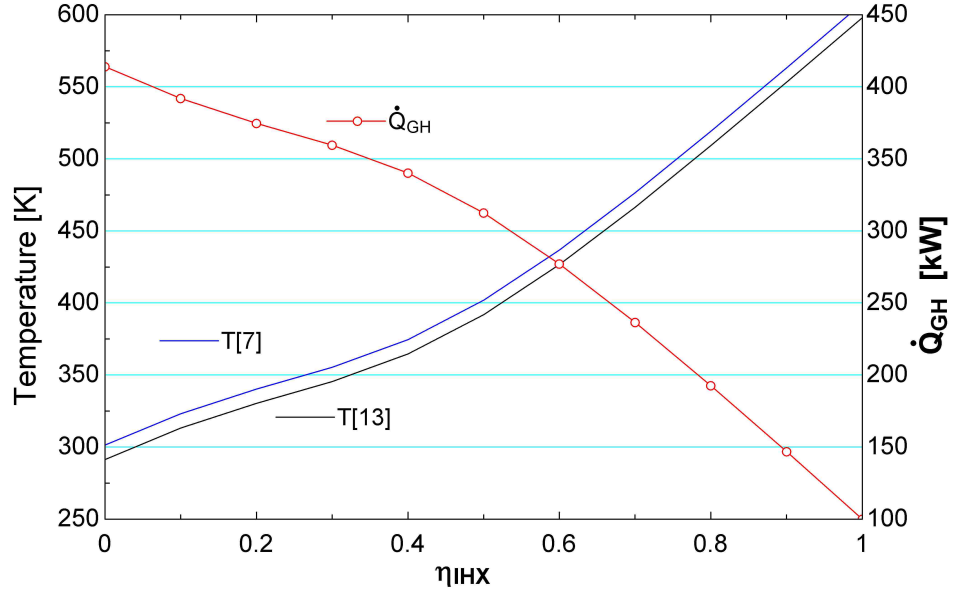

Figure 14: Effect of IHX effectiveness on gas heater parameters

Figure 14 shows how the quantity of heat transfer within the gas heater and the temperatures at state 7 and state 13 change with the internal heat exchanger effectiveness. The scale on the right is the amount of heat transfer in the gas heater and the scale on the left is the temperature for state 7 and state 13. Clearly the inclusion of an internal heat exchanger in the bottoming cycle reduces the amount of heat recovered from the topping cycle exhaust gas. In order to more effectively use the exergy of the exhaust gas, the remainder of the analysis is conducted using the alternate setup. Recall the alternate setup is a modification of the original which removes the the IHX and uses the condenser to produce domestic hot water.

### 4.2.1 Domestic Hot Water Production

To satisfy most hygienic needs, a domestic hot water temperature of 149 °F (65 °C) is commonly selected. For this section of the analysis, all of the input parameters are set to their nominal values and the domestic hot water at state 15 is held constant at 65 °C. Table 12 compares the results compared to average domestic requirements. The first row corresponds to the original scale with a topping cycle mass flow rate of 1.0 kg/s. To compare to average domestic requirements, the initial results are scaled down by a factor of 100. In summary, with a household fuel consumption of 690 grams of methane per hour, sufficient hot water (51.3 liter/hr) and sufficient power (3.89 kW) are produced simultaneously.

| | Air Flow Rate [kg/s] | Hot Water Temperature [C] | Hot Water Production [liter/hr] | Net Power [kW] | Fuel Consumption [kg/hr] |
|---|---|---|---|---|---|
| Original Scale | 1.00 | 65.0 | 5130 | 388.6 | 68.6 |
| 1/100 Scale | 0.0100 | **65.0** | **51.3** | **3.89** | 0.690 |
| Average Requirement Per Household | - | **65.0** | **45.0** | **1.39** | - |

Table 12: Domestic hot water production

### 4.2.1 Variation of Turbine Inlet Temperature

The TIT is varied from 1200-1500 K. Figure 15 shows the first law efficiencies for the Brayton cycle, the Rankine cycle, and the combined cycle versus TIT. Also shown is the exergetic efficiency of the combustor. The plot indicates that as TIT increases, all the energetic efficiencies increase. The Rankine cycle efficiency may appear quite low. This is because the cycle not only produces power but also hot water which is not accounted for in the energetic efficiency of a power cycle.

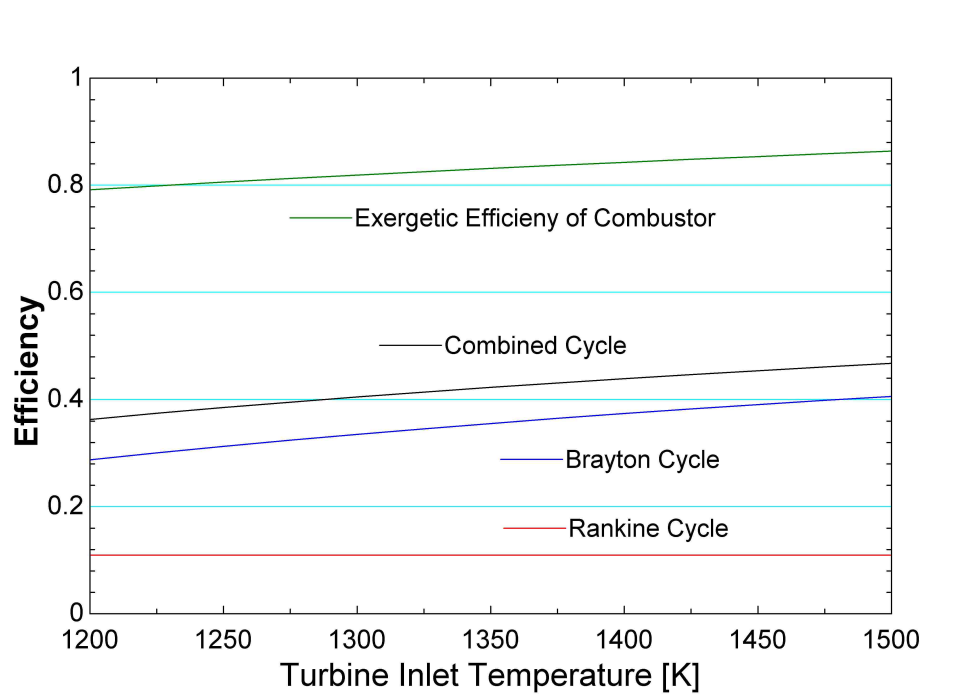

Figure 15: Efficiencies versus TIT

A surprising result is the exergetic efficiency of the combustor increases along with the turbine inlet temperature. This surprising result occurs because of the recuperator: the turbine exit temperature increases which therefore increases the combustor inlet temperature. With the average temperature in the combustor closer to the reservoir temperature, an increase in exergetic efficiency results.

Figure 16 shows the relative component-wise exergy destruction at TIT = 1200 K

and at TIT = 1500 K. The largest contribution to exergy destruction is the combustor. The total exergy destruction increases from 270 kJ/kg of air at TIT = 1200 K to 279 kJ/kg of air at TIT = 1500 K. The components that are most affected by a TIT increase are the combustor and condenser. The exergy destruction sensitivity in these components is intuitive because TIT directly affects the temperature gradients within them. Temperature gradients are direct sources of irreversibility.

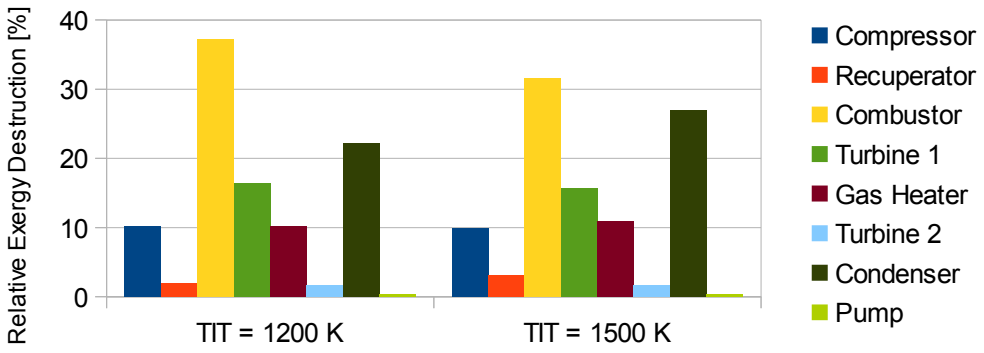


Figure 16: Relative exergy destruction versus TIT

### 4.2.2 Variation of Ambient Temperature

The ambient temperature is varied from 278 K (40.7 °F) to 302 K (83.9 °F). The rational for limiting the maximum temperature to 302 K is to allow for a 2 K temperature difference between the cooling water and the critical temperature of $CO_2$ in the condenser. At a temperature above 304 K leaving the condenser, the bottoming $CO_2$ cycle becomes entirely supercritical. Table 13 shows some relevant results for three of the

| Ambient Temperature | Condenser Pressure | $\eta_{1CC}$ | $\eta_{2CC}$ | Total Exergy Destruction |
|---|---|---|---|---|
| 278 [K] | 4.16 [MPa] | 51.4% | 62.2% | 235.8 [kJ/kg air] |
| 290 [K] | 5.58 [MPa] | 47.9% | 58.0% | 261.0 [kJ/kg air] |
| 302 [K] | 7.36 [MPa] | 44.1% | 53.3% | 288.5 [kJ/kg air] |

Table 13: Variation of ambient temperature

ambient temperatures tested. As the ambient temperature increases, the total exergy destruction and required condenser pressure increase. Also, an increase in ambient temperature results in a reduction in 1st and 2nd Law efficiencies.

### 4.2.3 Variation of Topping Cycle Pressure Ratio

The Brayton cycle pressure ratio is varied from 3 to 19. Turbine inlet temperature is preset to 1500 K. Figure 17 shows how the net specific work of the topping cycle (left) and the energetic efficiency (right) vary with topping cycle pressure ratio.

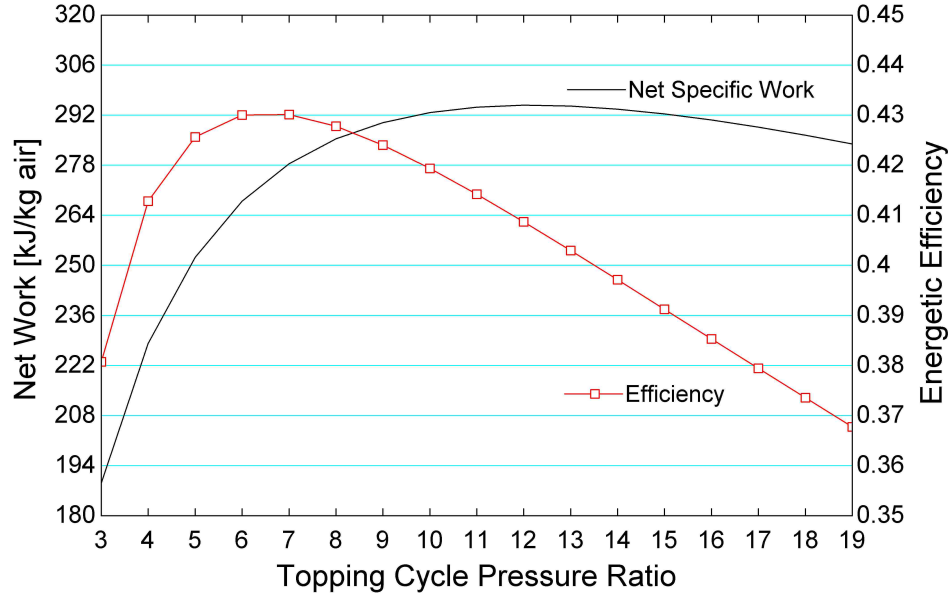


Figure 17: Topping cycle net specific work and efficiency versus pressure ratio

As was observed before, there does not exist a single pressure ratio which simultaneously maximizes net specific work and energetic efficiency. The maximum net power of the Brayton cycle is 295 kJ/kg air at a pressure ratio of 12.5. Figure 18 shows how the location of the maximum net specific work varies with pressure ratio and turbine 1 inlet temperature. The pressure ratio at which the maximum net specific work occurs decreases as turbine 1 inlet temperature decreases.

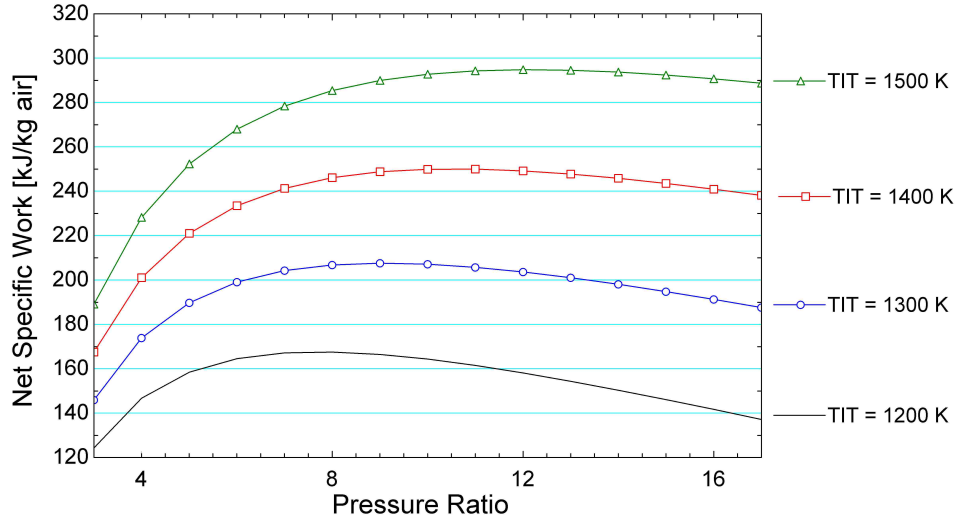


Figure 18: Effect of pressure ratio and TIT on the net specific work

For three different topping cycle pressure ratios, the exergy destruction in each component is shown in Figure 19. Relative exergy destruction in the recuperator, turbine 1, and condenser are most affected by a change in the Brayton cycle pressure ratio. With a higher pressure ratio results in more exergy destruction in turbine 1 because the turbine exit temperature is lower. This lower temperature leaving the turbine reduces the quantity

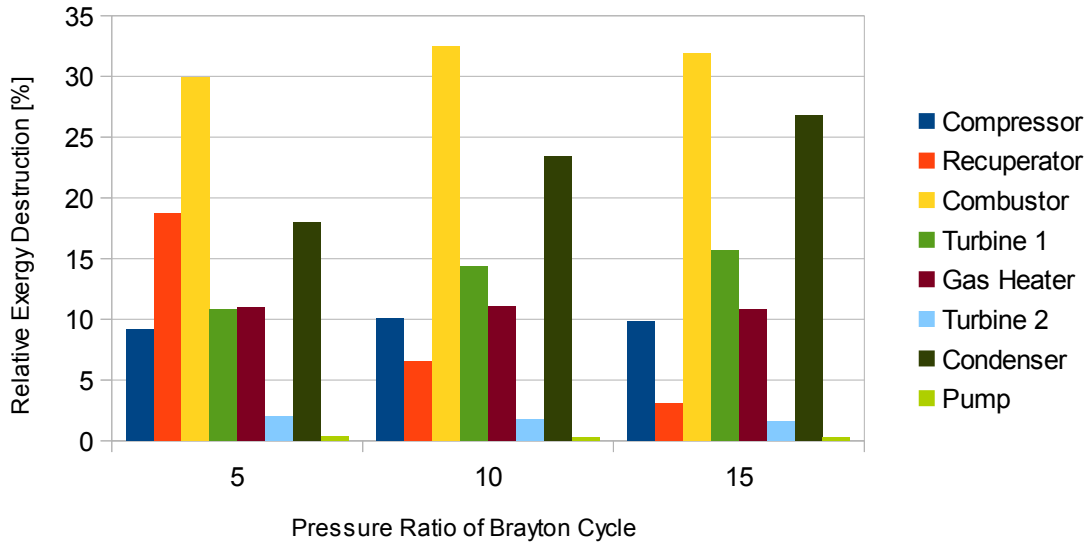


Figure 19: Relative exergy destruction versus pressure ratio

of heat transfer in the recuperator. The larger exergy destruction in the condenser is likely due to more heat being transferred into the bottoming cycle.

### 4.2.4 Variation of Recuperator Effectiveness

Recuperator effectiveness ($\eta_R$) is varied from 60% to an ideal 100%. Figure 20 plots the Brayton Cycle energetic efficiency (left), heat transfer in the gas heater (right), and recuperator heat transfer (right). Intuitively the amount of heat transfer in the recuperator increases with an increase in recuperator effectiveness. As a result, less heat is transferred into the bottoming cycle through the gas heater. Also, less heat is required from combustion. Maintaining power output while decreasing fuel utilization results in an increase of the topping cycle energetic efficiency to a maximum value of 44.2% with perfect recuperator effectiveness.

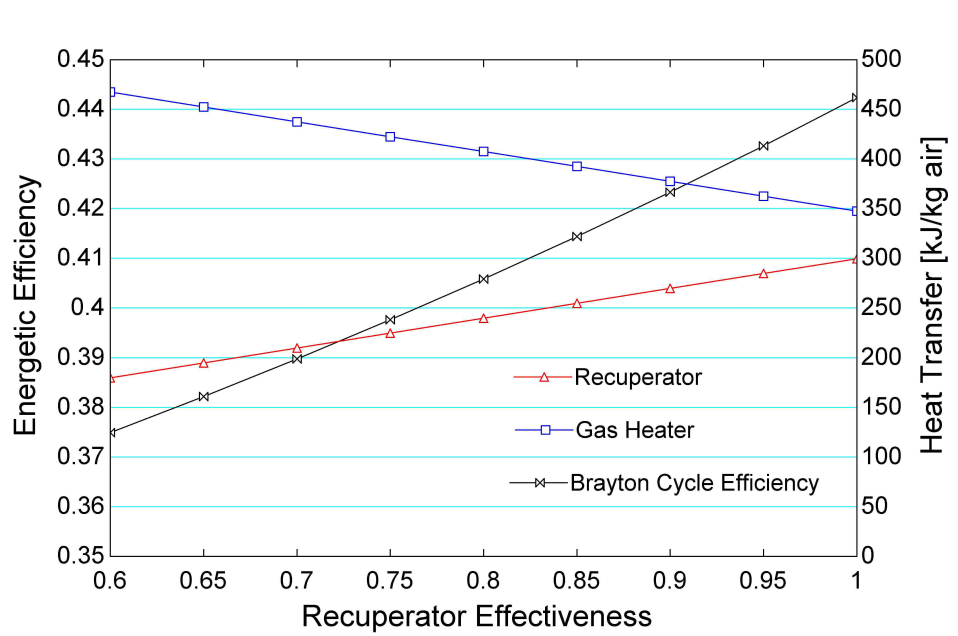

Figure 20: Topping cycle efficiency and heat transfer versus recuperator effectiveness

The relative component-wise exergy destruction with recuperator effectiveness set to 60 %, 80 % and 100 % is shown in Figure 21. Total Exergy destruction decreases from 305

kJ/kg of air at a recuperator effectiveness of 60 % to 221 kJ/kg of air with a perfect recuperator. Exergy destruction in the recuperator obviously decreases with a larger effectiveness. The relative exergy destructions in turbine 1 and the compressor appear to increase. This counter-intuitive result occurs because the actual exergy destruction in these components stay constant while the total exergy destruction decreases. The fraction of total exergy destroyed by these components therefore slightly increases. Exergy destruction in the condenser decreases with higher recuperator effectiveness because less heat is added to the bottoming cycle.

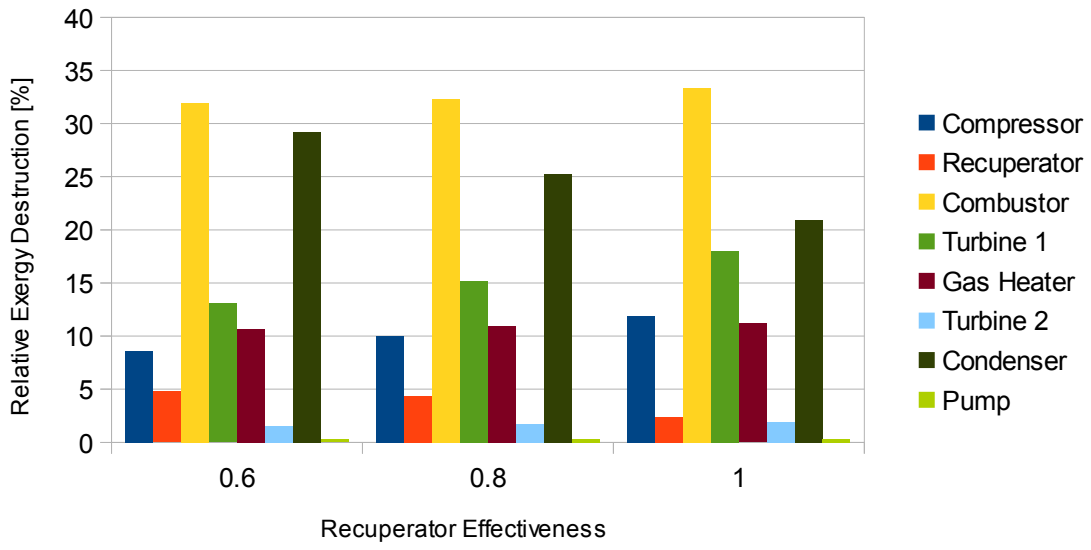


Figure 21: Relative exergy destruction versus recuperator effectiveness

### 4.2.5 Variation of Compressor/Pump Isentropic Efficiencies

For the parametric study of the pump and compressor isentropic efficiencies, the two values are set equal to each other and varied simultaneously. The most relevant output parameters are given in Table 14(a). An interesting observation is that the required heat from combustion increases as the pump and compressor efficiencies increase. This

occurs because the temperature at the outlets of these components decreases. The lower temperature entering the recuperator results in a slightly lower temperature leaving the recuperator. Consequently, more heat is required from combustion to raise the temperature to the desired turbine inlet temperature. Furthermore, the hot stream exits the recuperator slightly cooler which decreases heat transfer to the bottoming cycle via the gas heater. However, the benefit to the energetic efficiency of the combined cycle when increasing the pump and compressor efficiencies outweighs the slight increase in required combustion heat.

### 4.2.6 Variation of Turbine Isentropic Efficiencies

Like the parametric study for pump and compressor isentropic efficiencies, the

(a)

| $\eta_C$, $\eta_P$ | $\eta_{1CC}$ | Heat from Combustion [kJ/kg air] | Gas Heater Heat Transfer [kJ/kg air] | Total Exergy Destruction [kJ/kg air] |
|---|---|---|---|---|
| 75% | 41% | 716 | 446 | 300 |
| 80% | 44% | 722 | 426 | 281 |
| 85% | 47% | 726 | 407 | 264 |
| 90% | 49% | 730 | 391 | 249 |
| 95% | 51% | 734 | 377 | 235 |
| 100% | 53% | 738 | 363 | 223 |

(b)

| $\eta_{T1}$, $\eta_{T2}$ | $\eta_{1CC}$ | Heat of Combustion [kJ/kg air] | Gas Heater Heat Transfer [kJ/kg air] | Total Exergy Destruction [kJ/kg air] | Recuperator Heat Transfer [kJ/kg air] | Turbine 1 Exit Temperature [K] |
|---|---|---|---|---|---|---|
| 70% | 34% | 632 | 431 | 306 | 334 | 1036 |
| 75% | 39% | 664 | 423 | 292 | 303 | 1002 |
| 80% | 43% | 695 | 415 | 277 | 271 | 967 |
| 85% | 47% | 726 | 408 | 263 | 240 | 933 |
| 90% | 50% | 758 | 400 | 249 | 208 | 898 |
| 95% | 54% | 789 | 392 | 235 | 177 | 863 |
| 100% | 56% | 820 | 384 | 222 | 146 | 827 |

Table 14: Results of parametric study due to the (a) pump and compressor efficiencies and (b) turbine efficiencies

turbine isentropic efficiencies are set equal and varied simultaneously. At various turbine isentropic efficiencies, Table 14(b) shows the turbine exit temperature for the topping cycle, recuperator heat transfer, heat of combustion, heat transfer in the gas heater, combined cycle energetic efficiency, and total system exergy destruction. The turbine exit temperature decreases as the isentropic efficiency improves. A reduction in turbine inlet temperature reduces the recuperator heat transfer which consequently reduces the turbine inlet temperature. The reduction in turbine inlet temperature requires more heat from combustion. As with the pump and compressor isentropic efficiencies, a benefit to the combined cycle efficiency outweighs the increase in heat from combustion.

### 4.2.7 Variation of Gas Heater Temperature Differences

The gas heater hot side temperature difference is varied from 10-40 K. The results for increments of 10 K are shown in Table 15. The increase in temperature difference results in lower heat transfer rate in the gas heater which leads to less turbine power. The larger temperature difference present in the gas heater incurs more exergy destruction and thus a lower exergetic efficiency for the gas heater. A less expected result is the effect on the condenser: A lower turbine exit temperature reduces the temperature difference in the condenser, reducing the condenser exergy destruction and improving the condenser exergetic efficiency. Also, the volumetric flow rate of domestic hot water (149 °F) is reduced as a result of a smaller heat transfer rate in the gas heater.

| $\Delta T_{HOT}$ [K] | Rankine Cycle Net Work [kJ/kg air] | Gas Heater Heat Transfer [kJ/kg air] | Flow Rate Hot Water [liter/hr] | Gas Heater Exergetic Efficiency | Condenser Exergetic Efficiency | Gas Heater Exergy Destruction [kJ/kg air] | Condenser Exergy Destruction [kJ/kg air] |
|---|---|---|---|---|---|---|---|
| 10 | 44.6 | 408 | 9085 | 82.6% | 22.9% | 28.7 | 66.5 |
| 20 | 43.7 | 400 | 8903 | 79.8% | 23.5% | 33.4 | 63.1 |
| 30 | 42.9 | 392 | 8721 | 77.0% | 24.1% | 38.0 | 59.8 |
| 40 | 42.0 | 383 | 8540 | 74.2% | 24.8% | 42.6 | 56.5 |

Table 15: Variation of gas heater hot side temperature difference

The state present at the bottoming cycle inlet to the gas heater (State 13) is determined solely by the pump and condenser parameters. Therefore, altering the gas heater cold side temperature difference only has an affect on State 7. A variation of the exhaust temperature of State 7 only has an effect on the combined cycle exergetic efficiency. The effect however, is a magnitude on the order of 0.1%.

### 4.2.8 Variation of Bottoming Cycle Maximum Pressure

The maximum pressure in the bottoming Rankine cycle is varied from 10 MPa to 20 MPa. The minimum pressure is determined by the temperature of saturated $CO_2$ leaving the condenser. For this analysis, the temperature is set to 280 K which has a corresponding saturation pressure of 4.161 MPa. The pressure ratio was therefore varied from 2.40 to 4.81. The exergy destruction in the bottoming cycle components for three max cycle pressures is shown in Figure 22.

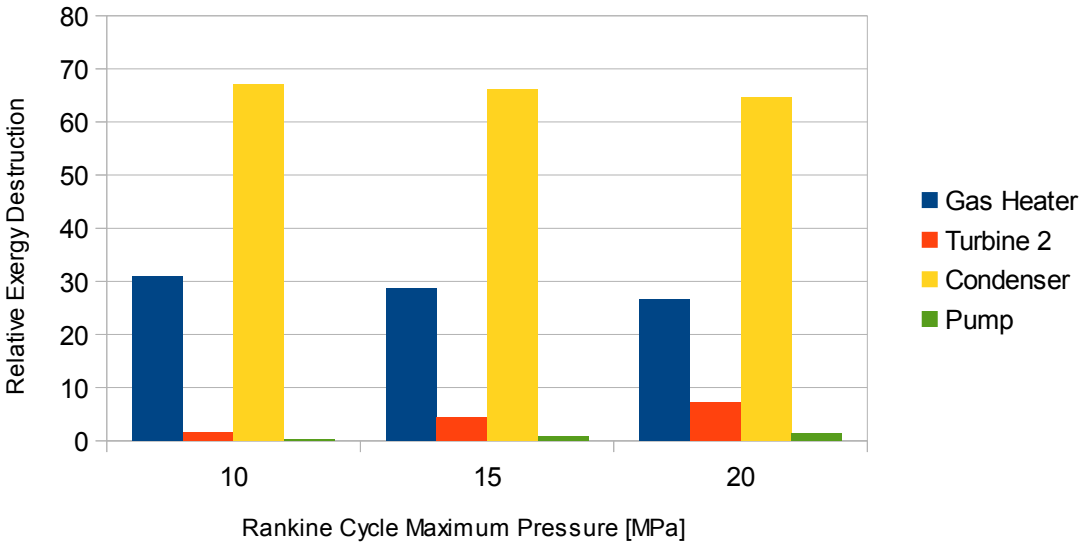


Figure 22: Relative exergy destruction versus Rankine cycle maximum pressure

It is apparent from the figure that the pump and turbine exergy destruction are relatively

small. An increase in maximum cycle pressure results in the following trends: Gas heater exergy destruction, condenser exergy destruction and total exergy destruction are reduced. The exergy destruction in the turbine increases because an expansion device becomes less efficient at higher pressures ratios.

The 1st and 2nd Law efficiencies versus the bottoming cycle maximum pressure are presented in Figure 23. Also shown in the figure is the net specific work of the Rankine cycle. As the maximum cycle pressure increases, the exergetic and energetic efficiencies increase.

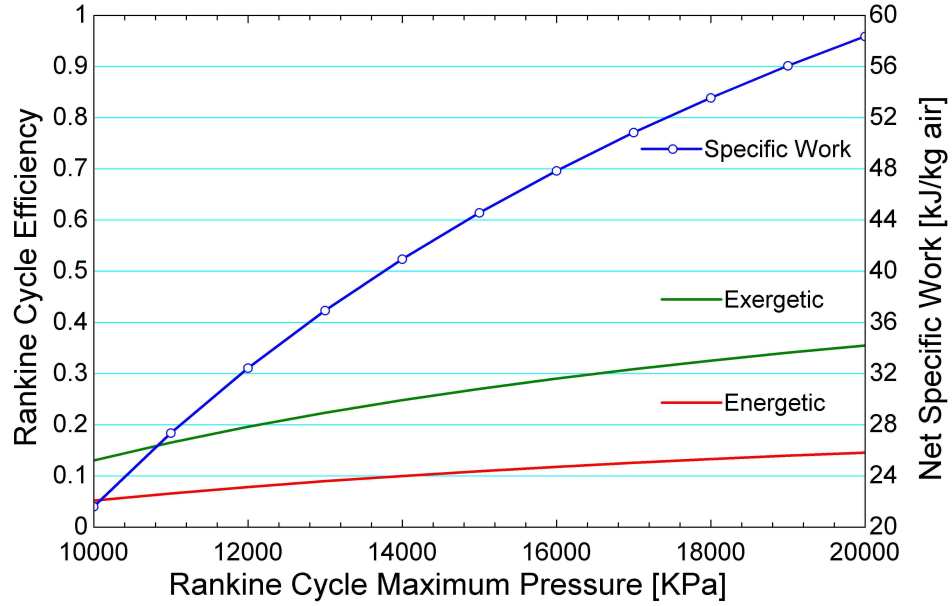

Figure 23: Rankine cycle efficiencies and specific work versus maximum cycle pressure

At the maximum tested pressure, the Rankine cycle energetic efficiency is 14.6 %. As mentioned previously, this may seem unreasonably low but the cycle is also producing domestic hot water which does not factor into the energetic efficiency. The positively sloped curve of efficiency versus maximum pressure suggests that the maximum efficiency is not within the tested pressure range. The maximum bottoming cycle

energetic efficiency is found to be 29.3 % at an unrealistic max cycle pressure of 110 MPa. In conclusion, the bottoming cycle maximum pressure should be as high as possible.

### 4.3 Relative Pressure Loss

Entropy change by a process may be written as,

$$dS = dS_e + dS_i \quad , \tag{6}$$

where $dS_e$ is the entropy change due to "external" effects in the form of heat transfer or work and $dS_i$ is the entropy change due to "internal" effects such as friction. The amount of internal irreversibility may be represented by "pressure loss". A pressure loss of zero describes a process without internal irreversibilities and thus no entropy change due to internal effects. By assuming no work or pressure loss, entropy change due to heat transfer may be approximated simply as the total entropy change. The approximation is most accurate for small pressure changes because $dS_e$ is a weak function of pressure change. Having isolated $dS_e$, solving for $dS_i$ is a trivial exercise. This method can also be adapted to the exergy balance.

A relative pressure loss factor, $\Delta F_P$, is used in the analysis. It is given by,

$$P_e = (1 - \Delta F_P) P_i \quad , \tag{7}$$

where $P_e$ is the exit pressure and $P_i$ is the inlet pressure. The analysis is conducted at relative pressure losses of 0, 2.5%, and 5%. To avoid interactions between components, one component is studied at a time with all other pressure losses set to a value of zero. Table 16 shows the component, its pressure loss, the resulting total component exergy destruction, exergy destruction due to friction, and 2nd Law efficiency. In accordance with

Equation 6, exergy destruction increases with an increase in frictional (pressure) losses.

The combustor and condenser are least sensitive to pressure loss with about 3 kJ/kg of air of exergy destruction due to friction at 5% pressure loss. The recuperator is the most sensitive to friction induced exergy destruction with a value of 9.5 kJ/kg of air at 5% pressure loss. It should be noted that the exergy destruction values for the recuperator, gas heater, and condenser are a sum of the two stream-wise exergy destructions within the component. Separation of the two stream-wise exergy destruction values is elusive because the proportion of irreversibility in each stream is determined by an approximated average temperature of heat transfer. To determine the stream-wise exergy destruction, a more detailed analysis can be performed using CFD calculations in the heat exchangers.

A pressure loss in one component also affects other components within the system. Further analysis is required to identify the behavior of these interactions. For the following results, actual exergy destruction rather than relative exergy destruction for each component is shown. Figure 24 shows the effect of component-wise exergy destruction with variation of relative recuperator pressure loss. With an increase in exergy

| Component | Relative Pressure Loss | Component Exergy Destruction [kJ/kg air] | Exergy Destruction due to Friction [kJ/kg air] | Component Exergetic Efficiency |
|---|---|---|---|---|
| Regenerator | 0.0% | 5.5 | 0.0 | 96.1% |
| | 2.5% | 10.1 | 4.7 | 93.1% |
| | 5.0% | 14.9 | 9.5 | 90.4% |
| Combustor | 0.0% | 86.3 | 0.0 | 86.5% |
| | 2.5% | 87.6 | 1.4 | 86.2% |
| | 5.0% | 89.0 | 2.8 | 85.9% |
| Gas Heater | 0.0% | 24.8 | 0.0 | 84.5% |
| | 2.5% | 27.9 | 3.1 | 82.8% |
| | 5.0% | 31.1 | 6.3 | 81.2% |
| Condenser | 0.0% | 61.6 | 0.0 | 23.9% |
| | 2.5% | 63.4 | 1.7 | 23.5% |
| | 5.0% | 65.2 | 3.5 | 23.0% |

Table 16: Variation of relative pressure loss

destruction in the recuperator, the combustor and turbine 1 show a reduction in exergy destruction. This is likely due to less exergy entering these two downstream components.

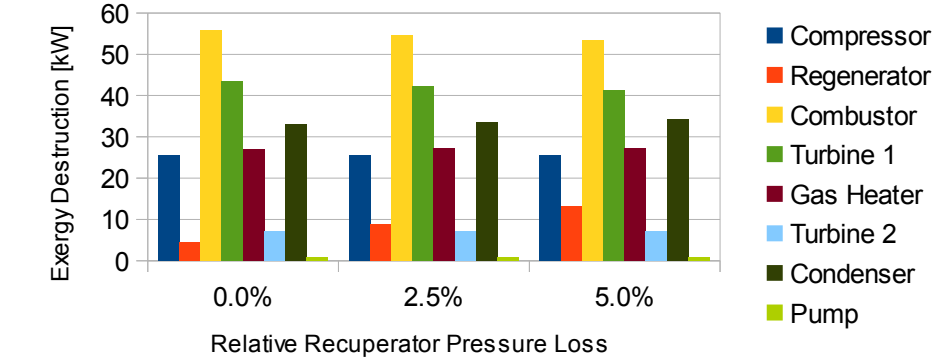


Figure 24: Actual exergy destruction for 3 recuperator pressure losses

As mentioned above, pressure loss variation in the combustor has relatively negligible effect. This result occurs because the constant temperature of the combustor exit stream (1500K) reduces the impact of pressure loss on the stream's high exit enthalpy.

Figure 25 shows the affect of gas heater pressure loss on component-wise exergy destruction. An increase of pressure loss in the gas heater creates more exergy destruction

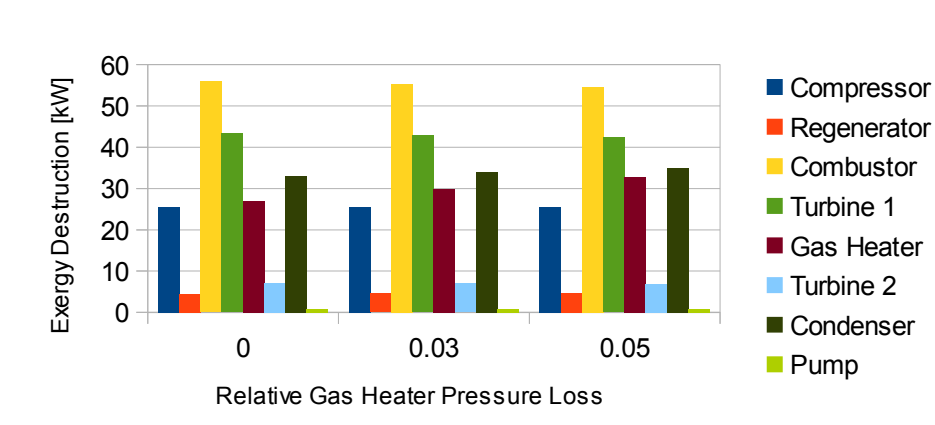


Figure 25: Component-wise exergy destruction for 3 GH pressure losses

in the condenser. This is due to a reduction of the expansion ratio in the bottoming cycle

turbine which results in a slightly higher turbine exit temperature. This increase in temperature at the condenser inlet creates a higher temperature gradient and thus more irreversibility in the condenser. A surprising consequence of an increase in gas heater pressure loss is the upstream affect. The Brayton side gas heater exit is discharged into atmospheric pressure. To counteract a pressure loss in the gas heater, a higher upstream pressure or “back pressure” occurs. The back pressure in the Brayton cycle slightly reduces the expansion ratio of the topping cycle turbine.

The only meaningful result of varying pressure loss in the condenser is the formation of a “back pressure” on the bottoming cycle turbine. Accordingly, a slight reduction in turbine work output is observed.

## 5.0 Conclusion and Future Work

Inclusion of an internal heat exchanger in the bottoming cycle is found to be ineffective in waste heat recovery. This is because an internal heat exchanger reduces the amount of heat transfer to the bottoming cycle. The excess heat is then just rejected to the environment which counteracts the whole purpose of including a bottoming power cycle for waste heat recovery. An alternative solution would be to keep the IHX and capture that excess heat with an additional bottoming cycle. Unfortunately, every subsequent bottoming cycle sees diminishing returns and at some point the capital cost outweighs the benefits. A better utilization of exergy is to produce domestic hot water in the condenser. On the scale of this theoretical system with a Brayton cycle mass flow rate of 1.0 kg/s, 100 homes can be supplied with sufficient power and hot water with a per household usage of about 700 grams of methane for each hour of operation.

Improving the topping cycle recuperator effectiveness makes the topping cycle more efficient in the sense that less heat is required from fuel. However, less heat is rejected to the bottoming cycle. A reduction in heat transfer from the topping cycle reduces the net power output of the bottoming cycle. For situations where increasing the recuperator effectiveness is unrealistic, inclusion of a heat recovery bottoming cycle is effective.

The air-standard approach is compared to the dry product analysis and a 7-8 % difference in enthalpy is observed. A slight overestimation of combined cycle 1$^{st}$ Law efficiency is likely. For computational simplicity, the air-standard approach was used. A dry product analysis, or better yet a CFD analysis with combustion, may be conducted in the future to produce more accurate results.

For turbine inlet temperature of 1500 K and a combustor inlet temperature of 300

K, a combustor irreversibility of about 30 % is achieved with a thermal reservoir temperature of 2100 K. An increase in the turbine inlet temperature does increase combustor irreversibility but raises the system efficiency.

Increasing the ambient temperature intuitively reduces the overall efficiency because of a decrease in the Carnot efficiency. Due to carbon dioxide's critical temperature near ambient temperature, the bottoming cycle is more sensitive to change in ambient temperature. The saturation temperature and pressure of carbon dioxide are related to the ambient temperature through the condenser temperature difference. Special attention must be given to the condensation temperature because if it exceeds 31 °C, the heat rejection process because supercritial. This has a primary affect on the bottoming cycle pressure ratio which is related to pump and turbine power.

Increasing the bottoming cycle max pressure increases the energetic efficiency and reduces exergy destruction. The maximum net power occurs at an extremely high pressure on the order of 110 MPa. Current material properties limit the max pressure to about 20 MPa.

For the configuration studied, a maximum topping cycle net work occurs at a Brayton cycle pressure ratio of 12.5. Above a pressure ratio of 12.5, the incremental power increase of the compressor begins to exceed that for the turbine. It should be noted that this is the result for a topping cycle without intercooling and reheat.

Increases of pressure losses within components have two major disadvantages. First, increased pressure loss increases the change in entropy and entropy production. This increase in entropy production translates to exergy destruction. Second, work potential is reduced because the creation of back pressures throughout the cycle reduce

expansion ratios in the turbines.

# Appendix A: Air-Standard Comparison EES Program

```
"Air-Standard Approximation Validation"
"EES Program for Master's Thesis"
"Robert S. Cordova, University of New Mexico"

"Inputs"
T_ref = 298 {K; reference temperature}
T_inlet = 500 {K; combustor inlet temperature}
T_exit = 1500 {K; combustor product exit tempeature}
//lamda = 2.03{Fuel Equivalence Ratio; e.g. 1 = 100% Theoretical Air}
P_ref = 101.3 {kPa; reference pressure}
P_R_B = 10 {Cycle Pressure Ratio}
P_inlet = P_ref*P_R_B {kPa; combustor pressure}
dP = 0.03 {relative pressure drop through combustor}
P_exit = (1-dP)*P_inlet

"Adiabatic Flame Temperature for methane combustion in given Fuel Equivalence Ratio(lamda)"
"Stoichiometric  Equation; CH4(g) +3(O2 + 3.76N2) --> CO2 + 2H2O + O2 + 11.28N2"

"Molar Flow Rates"
n_CH4r = 1 {kmol/s; Methane reactant}
n_O2r = lamda*2[kmol/s] {Oxygen reactant}
n_N2r = lamda*7.52[kmol/s] {Nitrogen reactant}
n_CO2p = 1 {kmol/s; CO2 product}
n_H2Op = 2 {kmol/s; Steam product}
n_O2p = (lamda - 1)*2[kmol/s] {Oxygen product}
n_N2p = n_N2r {Nitrogen product}
n_total = n_CH4r + n_O2r + n_N2r {kmol/s; total molar flow rate}
n_dot_exit = n_total
n_dot_fuel = n_CH4r
n_dot_inlet = n_dot_exit - n_dot_fuel

"Mole Fractions"
y_CH4r = n_CH4r/n_total
y_O2r = n_O2r/n_total
y_N2r = n_N2r/n_total
y_CO2p = n_CO2p/n_total
y_H2Op = n_H2Op/n_total
y_O2p = n_O2p/n_total
y_N2p = n_N2p/n_total

"State Molar Enthalpies"
h_bar_CH4r = h_bar_CH4_formation + (enthalpy(CH4, T = T_inlet) - enthalpy(CH4, T=T_ref)) {kJ/kmol}
h_bar_O2r = (enthalpy(O2, T=T_inlet ) - enthalpy(O2, T=T_ref)) {kJ/kmol}
h_bar_N2r = (enthalpy(N2, T=T_inlet) - enthalpy(N2, T=T_ref)) {kJ/kmol}
h_bar_CO2p = h_bar_CO2_formation + (enthalpy(CO2, T=T_flame) - enthalpy(CO2, T=T_ref))
{kJ/kmol}
h_bar_H2Op = h_bar_H2O_formation + (enthalpy(H2O, T=T_flame) - enthalpy(H2O, T=T_ref))
{kJ/kmol}
h_bar_O2p = (enthalpy(O2, T=T_flame) - enthalpy(O2, T=T_ref)) {kJ/kmol}
h_bar_N2p = (enthalpy(N2, T=T_flame) - enthalpy(O2, T=T_ref)) {kJ/kmol}

"Molar Enthalpies of Formation"
h_bar_CH4_formation = -74850 {kJ/kmol}
```

```
h_bar_H2O_formation = -241820 {kJ/kmol}
h_bar_CO2_formation = -393520 {kJ/kmol}

"Enthalpy Balance"
H_r = (n_CH4r*h_bar_CH4r) + (n_O2r*h_bar_O2r) + (n_N2r*h_bar_N2r) {kW}
H_p = (n_CO2p*h_bar_CO2p) + (n_H2Op*h_bar_H2Op) + (n_O2p*h_bar_O2p) + (n_N2p*h_bar_N2p)
{kW}
H_r = H_p
"Combustion Analysis"

"Mixture Heat of Combustion"
H_exit_mixture = n_CO2p*(enthalpy(CO2, T=T_exit) - enthalpy(CO2, T=T_ref)) +
n_H2Op*(enthalpy(H2O, T=T_exit) - enthalpy(H2O, T=T_ref)) + n_O2p*(enthalpy(O2, T=T_exit) -
enthalpy(O2, T=T_ref)) + n_N2p*(enthalpy(N2, T=T_exit) - enthalpy(N2, T=T_ref)) {kW}
H_inlet_mixture = n_CH4r*(enthalpy(CH4, T=T_inlet) - enthalpy(CH4, T=T_ref)) + n_O2r*(enthalpy(O2,
T=T_inlet) - enthalpy(O2, T=T_ref)) + n_N2r*(enthalpy(N2, T=T_inlet) - enthalpy(N2, T=T_ref)) {kW}
delta_H_mixture = (H_exit_mixture - H_inlet_mixture)*convert([kW],[MW]) {mW}

"Air-Standard Heat of Combustion"
H_exit_air = n_total*(enthalpy(Air, T=T_exit) - enthalpy(Air, T=T_ref)) {kW}
H_inlet_air = n_total*(enthalpy(Air, T=T_inlet) - enthalpy(Air, T=T_ref)) {kW}
delta_H_air = (H_exit_air - H_inlet_air)*convert([kW],[MW]) {MW}

"Comparison"
LHV = MolarMass(CH4)*convert([g/gmol],[kg/kmol])*50.02 [MJ/kg] {MJ/kmol; Lower Heating Value of
methane}
E_bar_chemical = 824350 [kJ/kmol] {Molar Chemical Exergy of methane}
delta_H_relative = 100[percent]*(delta_H_mixture - delta_H_air)/delta_H_mixture {relative difference of
heating values between mixture and air-standard analysis}

"Entropy Production"
S_dot_in = S_dot_CH4r + S_dot_O2r + S_dot_N2r {kW/K}
S_dot_CH4r = n_CH4r*(entropy(CH4, T=T_inlet, P=P_inlet*y_CH4r) - entropy(CH4, T=T_ref,
P=P_ref*y_CH4r)) {kW/K}
S_dot_O2r = n_O2r*(entropy(O2, T=T_inlet, P=P_inlet*y_O2r) - entropy(O2, T=T_ref, P=P_ref*y_O2r))
{kW/K}
S_dot_N2r = n_N2r*(entropy(N2, T=T_inlet, P=P_inlet*y_N2r) - entropy(N2, T=T_ref, P=P_ref*y_N2r))
{kW/K}
S_dot_out = S_dot_CO2p + S_dot_H2Op + S_dot_O2p + S_dot_N2p
S_dot_CO2p = n_CO2p*(entropy(CO2, T=T_flame, P=P_exit*y_CO2p) - entropy(CO2, T=T_ref,
P=P_ref*y_CO2p)) {kW/K}
S_dot_H2Op = n_H2Op*(entropy(H2O, T=T_flame, P=P_exit*y_H2Op) - entropy(H2O, T=T_ref,
P=P_ref*y_H2Op)) {kW/K}
S_dot_O2p = n_O2p*(entropy(O2, T=T_flame, P=P_exit*y_O2p) - entropy(O2, T=T_ref,
P=P_ref*y_O2p)) {kW/K}
S_dot_N2p = n_N2p*(entropy(N2, T=T_flame, P=P_exit*y_N2p) - entropy(N2, T=T_ref,
P=P_ref*y_N2p)) {kW/K}
Q_dot = delta_H_mixture*convert([MW],[kW]) {kW}
dS_e = -Q_dot/T_flame
sigma_dot =" -dS_e" - S_dot_in + S_dot_out

"Exergy Destruction"
E_dot_Destroyed = T_ref*sigma_dot
E_D_relative = E_Dot_Destroyed/(E_bar_chemical*n_CH4r)
```

# Appendix B: Combined Cycle EES Program

```
"Second Law Analysis of a Waste Heat Recovery Combined Power Cycle"
"EES Program for Master's Thesis"
"Robert S. Cordova, University of New Mexico"

"Component Efficiencies"
eta_R = 0.80 {Brayton recuperator effectiveness}
eta_C = 0.85 {Brayton compressor isentropic efficiency}
eta_T1=0.85 {Brayton turbine isentropic efficiency}
eta_T2 = 0.85 {Rankine turbine isentropic efficiency}
eta_P = 0.9{Rankine pump isentropic efficiency}

"Pressure Parameters"
P_ref = 101.3 {kPa; reference pressure}
P_r_B = 15 {Brayton cycle pressure ratio}
P_max =15000 {kPa; maximum pressure in Rankine cycle based on material limitations}
P_r_R = P_max/P_min {Resulting Rankine cycle pressure ratio}

"Mass Flow Rate"
m_dot_B = 1 {kg/s; mass flow rate of Brayton cycle}
//m_dot_R = 0.6464 [kg/s]

"Temperature Parameters"
T_ref = 278 {K; reference temperature}
T_reservoir = 2100 [K] {K; assigned temperature of thermal reservoir for combustion}
T_Ti = 1500 {K; turbine inlet temperature based on material limitations}
T_domestic = 338 {K; domestic hot water at 149F (65C)}
dT_hot = 10 {K; temperature difference between hot stream inlet and cold stream exit of gas heater}
dT_cold = 5{K; temperature difference between hot stream exit and cold stream inlet  of gas heater}
dT_minCOND = 2 {K; condenser approach temperature temperature}
T_reactants = T[3] {K; combustor inlet temperature}

"Component Relative Pressure Losses"
dP_reg = 0.03 {relative pressure drop in recuperator}
dP_comb = 0.03{relative pressure drop in combustor}
//dP_brGH = 0.03 {relative pressure drop in Brayton side gas heater}
//dP_raGH = 0.03 {relative pressure drop in Rankine side gas heater}
dP_brGH = dP_GH
dP_raGH = dP_GH
dP_GH = 0.03
dP_cond = 0.03 {relative pressure drop in condenser}

////////////////////////////////////////////////////////////////////////////
"BRAYTON TOPPING CYCLE"
////////////////////////////////////////////////////////////////////////////

"State 0: Brayton Cycle Dead State"
T[0] = T_ref
P[0] = P_ref
h_0_B = enthalpy(air,T=T[0]) {kJ/kg; Brayton cycle enthalpy at dead state}
s_0_B = entropy(air,T=T[0], P=P[0]) {kJ/kg-K; Brayton cycle entropy at dead state}

"State 1:Brayton cycle inlet before compression"
T[1] = T[0]
P[1] = P[0]
```

```
h[1] = h_0_B
s[1] = s_0_B
e[1] =  h[1] - h_0_B - T[0]*(s[1] - s_0_B ) {kJ/kg; specific exergy flow}

"State 2: after compression before entering cold stream side of recuperator"
P[2] = P[1] *P_r_B {kPa}
hs_2 = enthalpy(air, P=P[2], s=s[1]) {kJ/kg}
eta_C = (hs_2 - h[1])/(h[2] - h[1]) {definition of isentropic efficiency used to find h[2]}
T[2] = temperature(air, h=h[2]) {K}
s[2] = entropy(air, P=P[2], h=h[2]) {kJ/kg-K}
e[2] =  h[2] - h_0_B- T[0]*(s[2] - s_0_B ) {kJ/kg; specific exergy flow}

"State 3: after preheat before entering combustor"
P[3] = (1 - dP_reg)*P[2] {pressure drop through recuperator}
eta_R = (h[3] - h[2] )/(h[5] - h[2]) {definition of isentropic efficiency used to find h[3]}
T[3] = temperature(air, h=h[3]) {K}
s[3] = entropy(air, P=P[3], h=h[3]) {kJ/kg-K}
e[3] =  h[3] - h_0_B - T[0]*(s[3] - s_0_B ) {kJ/kg; specific exergy flow}

"State 4: after combustion, also turbine inlet state"
P[4] = (1-dP_comb)*P[3] {pressure drop through combustor}
T[4] = T_Ti
h[4] = enthalpy(air,T=T[4]) {kJ/kg}
s[4] = entropy(air,T=T[4], P=P[4]) {kJ/kg-K}
e[4] =  h[4] -h_0_B - T[0]*(s[4] - s_0_B )  {kJ/kg; specific exergy flow}

"State 5: after expansion in turbine before entering recuperator"
P[5] = P[7]/((1 - dP_reg)*(1 - dP_brGH)) {pressure before losses in gas heater and recuperator}
hs_5 = enthalpy(air, s=s[4], P=P[5]) {kJ/kg}
eta_T1 = (h[4] - h[5])/(h[4] - hs_5) {definition of isentropic efficiency used to find h[5]}
T[5] = temperature(air, h=h[5]) {K}
s[5] = entropy(air, P=P[5], h=h[5]) {kJ/kg-K}
e[5] =  h[5] - h_0_B- T[0]*(s[5] - s_0_B ) {kJ/kg; specific exergy flow}

"State 6: after leaving recuperator"
P[6] = P[7]/(1 - dP_brGH) {pressure before drop in gas heater}
h[6] = h[5] -h[3] +h[2] {kJ/kg; energy balance for recuperator}
T[6] = temperature(air,h = h[6]) {K}
s[6] = entropy(air, P=P[6], h = h[6]) {kJ/kg-K}
e[6] =  h[6] -h_0_B- T[0]*(s[6] - s_0_B ) {kJ/kg; specific exergy flow}

"COMPONENT EQUATIONS"

"Compressor"
W_dot_C = m_dot_B*(h[2] - h[1]) {kW; shaft work into compressors}
E_dot_Dcomp = W_dot_C +m_dot_B*(e[1] - e[2]) {KW; rate of exergy destruction in compressor}
epsilon_comp = m_dot_B*(e[2] - e[1])/W_dot_C {second law efficiency of compressor}

"recuperator"
Q_dot_reg = m_dot_B*(h[3] - h[2]) {kW; heat transferred into colder fluid in recuperator}
E_dot_Dreg= m_dot_B*(e[2] +e[5] - e[3] - e[6]) {kW; rate of exergy destruction in recuperator}
sigma_dot_reg = E_dot_Dreg/T_ref {kW/K; rate of entropy production in recuperator}
epsilon_reg = (e[3] -e[2])/(e[5] - e[6]) {second law efficiency of recuperator}

"Combustor"
Q_dot_comb = m_dot_B*(h[4] - h[3]) {kW; heat from combustion}
```

```
E_dot_Dcomb = (1-(T[0]/T_reservoir))*Q_dot_comb +m_dot_B*(e[3] - e[4]) {kW; rate of exergy destruction in combustor}
Sigma_dot_comb = E_dot_Dcomb/T_ref {kW/K; rate of entropy production in combustor}
epsilon_comb = m_dot_B*(e[4] - e[3])/((1-T[0]/T_reservoir)*Q_dot_comb) {second law efficiency of combustor}

"Brayton Turbine"
W_dot_T1 = m_dot_B*(h[4] - h[5]) {kW; shaft work produced by turbine}
E_dot_Dturb = -W_dot_T1 +m_dot_B*(e[4] - e[5]) {kW; rate of exergy destruction in turbine}
epsilon_T1 = W_dot_T1/(m_dot_B*(e[4] -e[5])) {Brayton tubine effectiveness}

////////////////////////////////////////////////////////////////////////////////
"RANKINE BOTTOMING CYCLE"
////////////////////////////////////////////////////////////////////////////////

"Rankine Cycle Dead State"
h_0_R = enthalpy(CarbonDioxide, P=P[0], T=T[0]) {kJ/kg; Rankine cycle dead state enthalpy}
s_0_R = entropy(CarbonDioxide, P=P[0], T=T[0]) {kJ/kg-K; Rankine cycle dead state entropy}

"Cooling Water Dead State"
h_0_C =  enthalpy(water, T=T[0], P=P[0]) {kJ/kg}
s_0_C = entropy(water, T=T[0], P=P[0]) {kJ/kg-K}

"State 11: leaving condenser as saturated liquid"
T[11] = T_ref + dT_minCOND {K; saturated liquid temperature}
P[11] = pressure(CarbonDioxide, T=T[11], x=0) {kPa; saturation pressure at T[11]}
P_min = P[11]
h[11] = enthalpy(CarbonDioxide, P=P[11], x = 0) {kJ/kg}
s[11] = entropy(CarbonDioxide, P=P[11], x = 0) {kJ/kg-K}
e[11] =  h[11] -h_0_R- T[0]*(s[11] - s_0_R ) {kJ/kg; specific exergy flow}

"State 12: after leaving pump, before entering IHX"
P[12] = P_max
hs_12 = enthalpy(CarbonDioxide, P=P[12], s=s[11]) {kJ/kg; isentropic enthalpy after pumping}
eta_P = (hs_12 - h[11])/(h[12] - h[11]) {pump isentropic efficiency}
T[12] = temperature(CarbonDioxide, P=P[12], h=h[12]) {K}
s[12] = entropy(CarbonDioxide, P=P[12], h=h[12]) {kJ/kg-K}
e[12] =  h[12] -h_0_R- T[0]*(s[12] - s_0_R ) {kJ/kg; specific exergy flow}

"State 13: equal to State 12 with IHX removed"
P[13] = P[12]
T[13] = T[12]
h[13] = h[12]
s[13] = entropy(CarbonDioxide, P=P[13], h=h[13]) {kJ/kg-K}
e[13] =  h[13] -h_0_R- T[0]*(s[13] - s_0_R ) {kJ/kg; specific exergy flow}

"State 8: after leaving gas heater, also turbine inlet state"
P[8] = (1 - dP_raGH)*P[13] {pressure drop through gas heater}
T[8] = T[6] - dT_hot {K; from specified temperature difference}
h[8] = enthalpy(CarbonDioxide, P=P[8], T=T[8]) {kJ/kg}
s[8] = entropy(CarbonDioxide, P=P[8], T=T[8]) {kJ/kg-K}
e[8] =  h[8] -h_0_R- T[0]*(s[8] - s_0_R ) {kJ/kg; specific exergy flow}

"State 9: after leaving turbine, before entering IHX"
P[9] = P[11]/(1-dP_cond) {pressure before drop in IHX}
hs_9 = enthalpy(CarbonDioxide, P=P[9] ,s = s[8]) {kJ/kg; Isentropic enthalpy after expansion}
```

```
eta_T2 = (h[8] - h[9])/(h[8] - hs_9) {definition of turbine isentropic efficiency used to determine h[9]}
T[9] = temperature(CarbonDioxide, P=P[9], h=h[9]) {K}
s[9] = entropy(CarbonDioxide, P=P[9], h=h[9]) {kJ/kg-K}
e[9] =  h[9] -h_0_R- T[0]*(s[9] - s_0_R ) {kJ/kg; specific exergy flow}

"State 10: equal to State 9 with IHX removed"
P[10] = P[9]
T[10] = T[9]
h[10] = h[9]
s[10] = entropy(CarbonDioxide, P=P[10], h=h[10]) {kJ/kg-K}
e[10] =  h[10] -h_0_R- T[0]*(s[10] - s_0_R ) {kJ/kg; specific exergy flow}

"State 7: exhaust gas leaving gas heater and Brayton cycle"
P[7] = P[0]
T[7] = T[13] + dT_cold {K; from specified temperature difference}
h[7] = enthalpy(Air, T=T[7]) {kJ/kg}
s[7] = entropy(Air, P=P[7],T=T[7]) {kJ/kg-K}
e[7] =  h[7] -h_0_B- T[0]*(s[7] - s_0_B ) {kJ/kg; specific exergy flow}

"State 14: cooling water inlet to condenser"
P[14] = P[0]/(1- dP_cond){pressure before entering condenser}
T[14] = T_ref
h[14] = enthalpy(water, T=T[14], P=P[14]) {kJ/kg}
s[14] = entropy(water, T=T[14], P=P[14]) {kJ/kg-s}
e[14] = h[14] - h_0_C -T[0]*(s[14] - s_0_C) {kJ/kg; specific exergy flow}

"State 15: domestic hot water leaving condenser"
P[15] = P[0] {kPa}
T[15] = T_domestic
h[15] = enthalpy(water, T=T[15], P=P[15]) {kJ/kg}
s[15] = entropy(water, T=T[15], P=P[15]) {kJ/kg-s}
e[15] = h[15] - h_0_C -T[0]*(s[15] - s_0_C) {kJ/kg; specific exergy flow}

"Rankine Cycle Mass Flow Rate"
m_dot_R = m_dot_B*((h[6] - h[7])/(h[8] - h[13])) {kg/s; Rankine cycle mass flow rate from energy
balance on gas heater}

"Domestic Hot Water Mass Flow Rate"
m_dot_h2o = m_dot_R*((h[10] - h[11] )/(h[15] - h[14])) {kg/s; domestic hot water mass flow rate from
energy balance on condenser}
V_bar_WATER = m_dot_h2o*volume(water, T=T_domestic, P=P_ref)*convert([m^3/s],[liter/hour])
{liters/hour; volumetric flow rate of dome tic hot water @ T_domestic}

"Gas Heater"
E_dot_Dgh = m_dot_B*(e[6] - e[7]) +m_dot_R*(e[13] - e[8]) {kW; exergy destruction in gas heater}
Q_dot_GH = m_dot_R*(h[8] - h[13]) {kW; heat transferred into Rankine cycle via gas heater}
Sigma_dot_GH = m_dot_B*(s[7] - s[6]) + m_dot_R*(s[8] - s[13]) {kW/K; rate of entropy production in
gas heater}
epsilon_GH = (m_dot_R*(e[8] - e[13]))/(m_dot_B*(e[6] - e[7])) {second law efficiency of gas heater}

"Rankine Turbine"
W_dot_T2 = m_dot_R*(h[8] - h[9]) {KW; shaft work from Rankine cycle turbine}
E_dot_Dturb2 = -W_dot_T2 +m_dot_R*(e[8] - e[9]) {kW; exergy destruction within Rankine cycle
turbine}
epsilon_T2 = W_dot_T2/(m_dot_R*(e[8] - e[9])) {Rankine turbine effectiveness}
```

```
"Pump"
W_dot_P = m_dot_R*(h[12] - h[11]) {kW; shaft work into pump}
E_dot_Dpump = W_dot_P +m_dot_R*(e[11] - e[12]) {kW; exergy destruction within pump}
epsilon_P = (m_dot_R*(e[12] - e[11]))/W_dot_P {second law efficiency of pump}

"Condenser"
Q_dot_cond = m_dot_R*(h[10] - h[11]) {kW; heat transferred out of working fluid within condenser}
E_dot_Dcond = m_dot_R*(e[10] - e[11]) +m_dot_h2o*(e[14] -e[15]) {kW; exergy destruction in
condenser}
epsilon_cond = (m_dot_h2o*(e[15] - e[14]))/(m_dot_R*(e[10] - e[11])) {exergetic efficiency of condenser}
sigma_dot_cond = E_dot_Dcond/T_ref {kW/K; rate of entropy production in condenser}

////////////////////////////////////////////////////////////////////////////
"FIGURES OF MERIT"
////////////////////////////////////////////////////////////////////////////

"Net Work"
W_dot_Bnet = W_dot_T1 - W_dot_C {kW; net work of Brayton cycle}
W_dot_Rnet = W_dot_T2 - W_dot_P {kW; net work of Rankine cycle}
W_dot_CCnet = W_dot_Bnet + W_dot_Rnet {kW; net work of Combined Cycle}

"Fuel Consumption"
LHV = 50020 [kJ/kg] {lower heating value}
m_dot_FUEL = m_dot_B*(e[4] - e[3])/(0.6*LHV) {kg/s; approximate mass flow rate of fuel based on 60%
exergy utilization in combustor}
lamda = (m_dot_B/m_dot_FUEL)/17.19 {approximate fuel equivalence ratio}

"Total Exergy Destruction"
E_Dtotal = E_dot_Dcomp + E_dot_Dreg +E_dot_Dcomb +E_dot_Dturb +E_dot_Dgh +E_dot_Dturb2
+E_dot_Dcond +E_dot_Dpump {kW}

"Relative Exergy Destruction"
RED_comp = 100*E_dot_Dcomp/E_Dtotal {relative exergy destruction in compressor }
RED_reg = 100*E_dot_Dreg/E_Dtotal {relative exergy destruction in recuperator }
RED_comb = 100*E_dot_Dcomb/E_Dtotal {relative exergy destruction in combustor}
RED_turb1 = 100*E_dot_Dturb/E_Dtotal {relative exergy destruction in turbine 1}
RED_gh = 100*E_dot_Dgh/E_Dtotal {relative exergy destruction in gas heater}
RED_turb2 = 100*E_dot_Dturb2/E_Dtotal {relative exergy destruction in turbine 2}
RED_cond = 100*E_dot_Dcond/E_Dtotal {relative exergy destruction in condenser}
RED_pump = 100*E_dot_Dpump/E_Dtotal {relative exergy destruction in pump}

"Carnot Efficiency"
eta_carnot = 1 - (T[0]/T_reservoir)
eta_improvement = (eta_1CC - eta_1B)/eta_1CC {relative energetic efficiency improvement with addition
of bottoming cycle}

"First Law Efficiencies"
"Brayton Cycle 1st Law Efficiency"
eta_1B = W_dot_Bnet/Q_dot_comb
"Rankine Cycle 1st Law Efficiency"
eta_1R = W_dot_Rnet/(Q_dot_GH)
"Combined Cycle 1st Law Efficiency"
eta_1CC = W_dot_CCnet/Q_dot_comb

"Second Law Efficiencies"
"Brayton Cycle"
```

```
E_dot_Bin = m_dot_B*(e[1] - e[6]) + (1 - (T[0]/T_reservoir))*Q_dot_comb {kW; exergy added}
E_dot_Bout = W_dot_Bnet {kW; exergy utilized}
eta_2B = E_dot_Bout/E_dot_Bin {exergetic efficiency of Brayton cycle}
"Rankine Cycle"
E_dot_Rin = m_dot_B*(e[6] - e[7])
E_dot_Rout = W_dot_Rnet
eta_2R = E_dot_Rout/E_dot_Rin

"Combined Cycle"
E_dot_in = m_dot_B*(e[1] - e[7]) +m_dot_h2o*(e[14] - e[15]) + (1 - (T[0]/T_reservoir))*Q_dot_comb
E_dot_out = W_dot_CCnet
eta_2CC = E_dot_out/E_dot_in

////////////////////////////////////////////////////////////////////////////////
"Balance Checks"
////////////////////////////////////////////////////////////////////////////////
Residual_energy = Q_dot_comb  - W_dot_CCnet + m_dot_B*( h[1] - h[7]) - m_dot_h2o*( h[15] - h[14])
{residual of energy balance, value of zero indicates proper balance}
Residual_exergy = (1- T[0]/T_reservoir)*Q_dot_comb - W_dot_CCnet + m_dot_h2o*(e[14] - e[15]) +
m_dot_B*(e[1] - e[7]) - E_Dtotal {residual of exergy balance, value of zero indicates proper balance}
```

## References


1. Austin, B.T.; Sumathy, K. Transcritical carbon dioxide heat pump systems: A review. *Renewable and Sustainable Energy Reviews* **2011**, *15*, 4013- 4029.
2. BCS Inc. *Waste Heat Recovery: Technology and Opportunities in the U.S. Industry.* U.S Department of Energy, 2008
3. Cayer, E.; Galanis, N.; Desilets, M.; Nesreddine, H.; Roy, P. Analysis of a carbon dioxide transcritical power cycle using a low temperature source. *Applied Energy* **2009**, *86*, 1055-1063.
4. Cayer, E.; Galanis, N.; Nesreddine, H. Parametric Study and Optimization of a Transcritical Power Cycle Using a Low Temperature Source. *Applied Energy* **2010**, *87*, 1249-1257.
5. Chacartegui, R.; Munoz de Escolona, J.M.; Sanchez, D.; Monje, B.; Sanchez, T. Alternative cycles based on carbon dioxide for central receiver solar power plants. *Applied Thermal Engineering* **2011**, *31*, 872-879.
6. Chen, Y.; Lundqvist, P.; Johansson, A.; Platell, P. A comparative study of the carbon dioxide transcritical power cycle compared with an organic Rankine cycle with R123 as working fluid in waste heat recovery. *Applied Thermal Engineering* **2006**, *26*, 2142-2147.
7. Chen, Y.; Lundqvist, P.; Platell, P. Theoretical research of carbon dioxide power cycle application in automobile industry to reduce vehicle's fuel consumption. *Applied Thermal Engineering* **2005** , *25*, 2041-2053.
8. Feher, E.G. The Supercritical Thermodynamic Power Cycle. *Energy Conversion* **1968**, *8*, 85-90.
9. Ganapathy, V. Heat-Recovery Steam Generators: Understand the Basics.

*Chemical Engineering* **1996**, *92*, 32-45.

10. Kehlhofer, R. *Combined-Cycle Gas and Steam Turbine Power Plants*; Penn Well Publishing Company: Tulsa, Oklahoma, 1997.
11. Kim, M-H.; Petterson, J.; Bullard, C.W. Fundamental process and system design issues in CO2 vapor compression systems. *Progress in Energy and Combustion Science* **2004**, *30,* 119-174.
12. Klein, S. A. *Engineering Equation Solver (EES) for Microsoft Windows Operating System: Academic Commercial* Version; F-Chart Software: Madison, WI, **2012** (available on the Web at http://www.fchart.com)
13. Marrero, I.O.; Lefsaker, A. M.; Razani, A; Kim, K.J. Second law analysis and optimization of a combined power cycle. *Energy Conversion and Management* **2002,** *43*, 557-573.
14. McQuay Air Conditioning. *Refrigerants Application Guide;* Technical Report No. AG 31-007, **2002**.
15. Moran, M.J.; Shapiro, H.N. *Fundamentals of Engineering Thermodynamics*,6th ed.; Jon Wiley & Sons, Inc.: New Jersey, **2008**.
16. Persichilli, M.; Kacludis, A.; Zdankiewicz, E.; Held, T. *Supercritical CO2 Power Cycle Developments and Commercialization: Why sCO2 can Displace Steam*, Proceedings from Power-Generation India & Central Asia Conference, Pragati Maidan, New Delhi India, April 19-21, **2012**.
17. Roy, J.P.; Mishra, M.K.; Misra, A. Parametric optimization and performance analysis of a waste heat recovery system using Organic Rankine Cycle. *Energy* **2010**, *35*, 5049-5062.

18. Siemens Energy. Combined Cycle site. http://www.energy.siemens.com/us/en/industries-utilities/power/processes/combined-cycle.htm (accessed 3/31/13).

19. Vaja, I.; Gamborotta, A. Internal Combustion Engine (ICE) bottoming with Organic Rankine Cycles (ORCs). *Energy* **2010**, *35*, 1084-1093.

20. Velez, F.; Segovia, J.; Chejne, F.; Antolin, G.; Quijano, A.; Martin, M.C. Low temperature heat source for power generation: Exhaustive analysis of a carbon dioxide transcritical power cycle. *Energy* **2011**, *26*, 5497-5507.

21. Velez, F.; Segovia, J.J.; Martin, M.C.; Antolin, G.; Chejn, F.; Quijano, A. Comparative study of working fluids for a Rankine cycle operating at low temperature. *Fuel Processing Technology* **2012**, *103*, 71-77.

22. Wright, S. Mighty Mite. *Mechanical Engineering*, [Online], January, **2012**. http://www.barber-nichols.com/sites/default/files/wysiwyg/images/supercritical_co2_turbines.pdf (accessed October, 2012).